Abstract

During the Last Interglacial (LIG, ~130–115 kiloyear (kyr) before present (BP)), the northern high latitudes were characterized by higher temperatures than those of the late Holocene and a lower Greenland Ice Sheet (GIS). However, the impact of a reduced GIS on the global climate has not yet been well constrained. In this study, we quantify the contribution of the GIS to LIG warmth by performing various sensitivity studies based on equilibrium simulations, employing the Community Earth System Models (COSMOS), with a focus on height and extent of the GIS. We present the first study on the effects of a reduction in GIS on the global surface temperature (TS) anomalies and separate the contribution of different forcings to LIG warmth. The strong Northern Hemisphere warming is mainly caused by increased summer insolation. Reducing the height by ~1300 m and the extent of the GIS does not have a strong influence during summer, leading to an additional warming of only +0.24°C. The effect of a reduction in GIS is strongest during local winter, with up to +5°C warming in the northern and southern high latitudes and an increase in global average temperature of +0.48°C. Furthermore, the method by which GIS configuration is changed influences the results.

In order to evaluate the performance of our LIG simulations, we additionally compare the simulated TS anomalies with marine and terrestrial proxy-based LIG temperature anomalies derived from three different proxy data compilations. Our model results are in good agreement with proxy records with respect to the warming pattern, but underestimate the reconstructed temperatures, suggesting a potential misinterpretation of the proxy records or deficits of our model such as low resolution, lack of biogeochemistry feedback, of lithosphere, or of a coupled ice sheet model). However, we are able to partly reduce the mismatch between model and data by additionally taking into account the potential seasonal bias of the proxy record and the uncertainties in the dating of the proxy records for the LIG thermal maximum. The seasonal bias and the uncertainty of the timing are estimated from our own transient model simulations covering the whole LIG (130–115 kyr BP). Changes in GIS improve the model-data agreement when annual mean proxies are considered rather proxies that record summer temperatures. Additionally, by comparing our model results to temperature reconstructions we can conclude that the GIS elevation was not as low as prescribed in our simulations, but potentially lower than prescribed in other studies. Thus, the question regarding the real size of the GIS during the LIG has yet to be answered.

1. Introduction

One important application of atmosphere–ocean general circulation models (AOGCMs) is the

computation of future climate projections (Collins et al., 2013; Kirtman et al., 2013). These projections allow insight into possible future climate states that may be notably different from present day. In order to ensure the reliability of such climate projections, the climate models' ability to replicate climate states that are different from the present needs to be tested (e.g. Braconnot et al., 2012; Flato et al., 2013) – this is necessary since model development is biased towards present climate states as a result of the tuning of various physical parameterizations towards modern observations. Past time periods provide the means for evaluating the performance of general circulation models (e.g. Dowsett et al., 2013; Lohmann et al., 2013; Lunt et al., 2013).

In particular, the simulation of interglacial climates provides an example of how models can respond when strong changes in the forcing are applied (Mearns et al., 2001). For a better understanding and assessment of potential future climate change it is necessary to analyze the main drivers leading to an interglacial climate that was warmer than the present interglacial. The Last Interglacial (LIG, ~130–115 kiloyear (kyr) before present (BP)) represents the penultimate interglacial before the Holocene (10–0 kyr BP), and is considered to be on average warmer than the Holocene (CLIMAP Project Members, 1984; Martinson et al., 1987; Kukla et al., 2002; Bauch and Erlenkeuser, 2003; Felis et al., 2004; Kaspar et al., 2005; Jansen et al., 2007; Turney and Jones, 2010; Masson-Delmotte et al., 2013). Model simulations indicate a pronounced warming during boreal summer in northern high latitudes (Harrison et al., 1995; Kaspar et al., 2005; Otto-Bliesner et al., 2006; Lohmann and Lorenz, 2007; Stone et al., 2013). Proxy records located in the Northern Hemisphere indicate also that LIG climate is characterized by temperatures that are several degrees Celsius above preindustrial (PI) values (Kaspar et al., 2005; CAPE Last Interglacial Project Members, 2006; Turney and Jones, 2010; Mckay et al., 2011). According to climate reconstructions, Arctic summer temperatures were about +2 to +4°C warmer than those of the late Holocene (CAPE Last Interglacial Project Members, 2006). Winter in high latitudes is considered to be warmer during the LIG due to sea ice feedbacks (Montoya et al., 2000; Kaspar et al., 2005; Yin and Berger, 2010). One cause for LIG warmth in summer was increased summer insolation at middle to high latitudes. Enhanced seasonality in the Northern Hemisphere is attributed to larger obliquity (ε) and eccentricity (e) relative to today (Berger, 1978), with Earth's orbital eccentricity being more than twice the PI value (Berger and Loutre, 1991), and boreal summer coinciding with the Earth passing the perihelion (Laskar et al., 2004; Yin and Berger, 2010). Greenhouse gas (GHG) concentrations during the LIG were similar to PI. Changes in the insolation forcing determine feedbacks in the ocean, atmosphere, vegetation, and sea ice, which

further influence the climate (e.g. Berger and Loutre, 1991; Braconnot et al., 2012).

According to different studies, the Greenland Ice Sheet (GIS) was lower during the LIG compared to PI, but the magnitude of reduction of elevation and area of the GIS has yet to be determined. Studies based on reconstructions and climate model simulations suggest a partial or complete absence of the GIS during the LIG, and that the sea level was higher than PI (Veeh, 1966; Stirling et al., 1998; Cuffey and Marshall, 2000; Otto-Bliesner et al., 2006; Overpeck et al., 2006; Jansen et al., 2007; Kopp et al., 2009, 2013; Alley et al., 2010; van de Berg et al., 2011; Robinson et al., 2011; Dutton and Lambeck, 2012; Dahl-Jensen et al., 2013; Quiquet et al., 2013; Church et al., 2013; Stone et al., 2013), while a more recent study based on ice core data proposes only a modest GIS change (i.e. equivalent to a contribution to sea level rise of ~2 m, Dahl-Jensen et al., 2013). An increase in sea level during the LIG as high as 8 m is proposed by Kopp et al. (2009) based on sea level data synthesis, which may imply a large contribution from the GIS and the Antarctic Ice Sheet. The contribution of a partially melted GIS to LIG sea level rise is not yet well determined; various studies suggest a sea level rise due to meltwater from Greenland of +0.3 to +5.5 m (Cuffey and Marshall, 2000; Tarasov and Peltier, 2003; Lhomme et al., 2005; Otto-Bliesner et al., 2006; Colville et al., 2011; Quiquet et al., 2013; Stone et al., 2013).

Existing studies on the effects of a reduced GIS during the LIG have been centered mostly on the Northern Hemisphere and focused on implications related to sea level rise (Stone et al. 2013) and Atlantic Meridional Overturning Circulation (AMOC) (Bakker et al. 2012). The studies by Bakker et al. (2012) and Stone et al. (2013) assume a relatively modest reduction of the GIS and find a mismatch between the simulated and the proxy-based temperature anomalies with respect to PI (CAPE Last Interglacial Project Members, 2006). Otto-Bliesner et al. (2006) find that a GIS elevation reduced by 500 m leads to a pronounced warming of up to +5°C in middle to high latitude summer. However, they find as well a mismatch between model and data, with the model underestimating the temperature anomaly indicated by the proxy record. In an LIG study based on transient climate model simulations performed with an earth system model of intermediate complexity, Loutre et al. (2014) find that changes in the Northern Hemisphere ice sheets configuration (extent and albedo) have only a small impact on the climate at the beginning of the LIG. They find as well an underestimation of the reconstructed temperatures by the model, even when taking into account several uncertainties. Bakker and Renssen (2014), who perform an analysis of transient simulations for the LIG, provide a partial explanation for the model-data mismatch, proposing that such large differences between the

reconstructed and simulated LIG temperatures may stem from the assumption in temperatures reconstructions that the LIG thermal maximum occurred synchronously in space and time. Their study suggests that global compilations of reconstructed LIG thermal maximum overestimate the warming.

Another model-data comparison study (Otto-Bliesner et al., 2013) for the LIG, based on an AOGCM (but with no changes in GIS elevation or extent) also shows an underestimation of global temperature reconstructions by Turney and Jones (2010) and McKay et al. (2011). Lunt et al. (2013) compare global terrestrial and marine proxy-based temperature anomalies with respect to PI by Turney and Jones (2010) to an ensemble of equilibrium simulations for the LIG performed with different state-of-the-art climate models. Even when considering a multi-model and a multi-proxy approach, they also find a pronounced disagreement between model and data, with the model underestimating the reconstructed temperature.The lack of accurate and independent age models for most paleoclimatic record during the LIG could be one cause for the observed model-data discrepancy (e.g. Drysdale et al., 2009; Govin et al., 2012; Capron et al., 2014). For example, the compilation of LIG temperature reconstructions included in this study (CAPE Last Interglacial Project Members, 2006) represents one single snapshot on the LIG thermal maximum, with the assumption that maximum warmth occurred synchronously across the globe. This assumption has to be made when compiling reconstructed LIG temperatures as it is difficult to align time series from different types of paleoclimatic archives since they do not benefit from robust absolute timescale allowing precise temporal comparison between different regions and between different archives (Capron et al., 2014).

Moreover, different studies (modelling as well as proxy-based) indicate that the maximum LIG warmth occurred at different times throughout the LIG in dependence of the geographical location (Bakker et al., 2012; Govin et al., 2012; Langebroek and Nisancioglu, 2014). Additionally, some proxy records may be seasonally biased (Lohmann et al., 2013, and references therein). Still, the models used by Lunt et al. (2013) and Otto-Bliesner et al. (2013) do not capture the magnitude of change recorded by the proxies, even when simulated summer mean temperature anomalies are considered.

Transient LIG climate simulations provide the possibility to determine when and where maximum LIG warmth occurred, and whether a given record may be seasonally biased or rather represents annual mean temperatures. Therefore, transient climate simulations may help to clarify the origin of the disagreement between model and data.In this study, we analyze the effect of a reduced GIS on LIG global climate with a focus on surface temperature (TS) at 130 kyr BP. The TS is derived from equilibrium simulations performed with the AOGCM COSMOS. We perform several sensitivity

simulations with different boundary conditions and use three different methods of reducing GIS elevation to half its preindustrial elevation and/or extent. This approach enables us to determine what GIS configuration has the strongest impact on the global temperature. Additionally, we assess the importance of additional forcings like insolation and albedo. Furthermore, in order to validate our results, we perform a model-data comparison using three different proxy-based temperature compilations by CAPE Last Interglacial Project Members (2006), Turney and Jones (2010), and Capron et al. (2014). For model-data comparison, we additionally consider the timing uncertainty of the maximum LIG warmth as determined from our transient simulations as well as the potential seasonal bias of the proxy record.

2. Data and methods

2.1 Model description

The Community Earth System Models (COSMOS) consist of the general atmosphere circulation model ECHAM5 (5th generation of the European Centre Hamburg Model; Roeckner et al., 2003), the land surface and vegetation model JSBACH (Jena Scheme of Atmosphere Coupling in Hamburg; Raddatz et al., 2007), the general ocean circulation model MPIOM (Max-Planck-Institute Ocean Model; Marsland et al., 2003), and the OASIS3 coupler (Ocean-Atmosphere-Sea Ice-Soil; Valcke et al., 2003; Valcke, 2013) that enables the atmosphere and ocean to interact with each other. COSMOS is mainly developed at the Max-Planck-Institute for Meteorology in Hamburg (Germany). The atmospheric component ECHAM5 is a spectral model, which is used in this study at a horizontal resolution of T31 (~3.75°×3.75°) with a vertical resolution of 19 hybrid sigma-pressure levels, the highest level being located at 10 hPa. The JSBACH simulates fluxes of energy, momentum, and CO_2 between land and atmosphere and comprises the dynamic vegetation module by Brovkin et al. (2009) which enables the terrestrial plant cover to explicitly adjust to variations in the climate state. MPIOM is formulated on a bipolar orthogonal spherical coordinate system. We employ it at a horizontal resolution of GR30 (corresponding to ~3°×1.8°) with 40 vertical levels. MPIOM includes a Hibler-type zero-layer dynamic-thermodynamic sea ice model with viscous plastic rheology (Semtner, 1976; Hibler, 1979). No flux correction is applied (Jungclaus et al., 2006). Model time steps are 40 min (atmosphere) and 144 min (ocean). This COSMOS configuration has been applied for the mid- and early Holocene (Wei and Lohmann, 2012), glacial conditions (Gong et al., 2013; Zhang et al., 2013, 2014), the Pliocene (Stepanek and Lohmann, 2012), the Miocene (Knorr et al., 2011; Knorr and Lohmann, 2014), future

climate projections (Gierz et al., 2015), and the LIG (Lunt et al., 2013; Pfeiffer and Lohmann, 2013; Bakker et al., 2014; Felis et al., 2015; Gong et al., 2015; Jennings et al., 2015).

2.2 Experimental setup

As control climate we use a PI simulation described by Wei et al. (2012). Greenhouse gas concentrations and astronomical forcing of the PI simulation are prescribed according to the Paleoclimate Modelling Intercomparison Project Phase 2 (PMIP2) protocol (Braconnot et al., 2007). Several equilibrium simulations covering the LIG are performed using fixed boundary conditions for 130 and 125 kyr BP time slices. The latter simulation is performed in order to assess whether a reduction in GIS at 125 kyr BP improves the model-data agreement. Astronomical parameters for the time slices considered in this study have been calculated according to Berger (1978) and are given in Table 1. It is known that one main driver for LIG climate is the Earth's astronomical parameters (Kutzbach et al., 1991; Crowley and Kim, 1994; Montoya et al., 2000; Felis et al., 2004; Kaspar and Cubasch, 2007). During the early part of the LIG, the axial tilt (obliquity) was higher which caused stronger summer insolation at high latitudes of the Northern Hemisphere, while the low latitudes received less insolation; this effect manifests in enhanced seasonality (i.e. warmer summers and cooler winters) in the early LIG climate. The Earth's orbital eccentricity was more than twice the present-day value (Berger and Loutre, 1991), and boreal summer coincided with the Earth passing the perihelion (Laskar et al., 2004; Yin and Berger, 2010).

Our main focus is the effects of height and extent of the GIS and of insolation changes on climate; consequently, GHG concentrations are prescribed at mid-Holocene levels (278 parts per million by volume (ppmv) CO_2, 650 parts per billion by volume 10 (ppbv) CH_4, and 270 ppbv N_2O, Table 1).. An additional simulation is performed using values for GHG concentrations proposed in the Paleoclimate Modelling Intercomparison Project Phase 3 (PMIP3) for the 130 kyr BP time slice (e.g. Lunt et al., 2012) and corresponding to 257 ppmv for CO_2, 512 ppbv for CH_4, and 239 ppbv for N_2O (LIG-GHG, Table 1, Fig. S1). This simulation is included in the Supplementary material as a control run for the GHG concentrations used in our LIG sensitivity simulations, in order to show that there is no large scale impact of lower GHG concentrations relative to our LIG control simulation (Fig. S1). Another LIG simulation is forced with increased CH_4 (760 ppbv) and slightly increased CO_2 (280 ppmv) in order to have one LIG simulation that has identical GHG concentrations to the ones prescribed in the PI simulation (Wei et al., 2012) (Table 1).

The size of the GIS during the LIG is not well constrained by reconstructions (Koerner, 1989;

Koerner and Fisher, 2002; NGRIP members, 2004; Johnsen and Vinther, 2007; Willerslev et al., 2007; Alley et al., 2010; Dahl-Jensen et al., 2013). We take this uncertainty into account and perform sensitivity simulations with three different elevations and two different ice sheet areas of the GIS (Fig. 1). An LIG simulation (LIG-ctl) with a preindustrial GIS elevation (Table 1, Fig. 1a) is used as control run for our LIG simulations, which allows us to quantify the exclusive effects of Greenland elevation on climate. Four simulations (Table 1) are performed using a modified GIS. We consider (1) a GIS lowered to half its present elevation (LIG-×0.5) with unchanged GIS area (Fig. 1b); (2) a GIS lowered by 1300 m (LIG-1300m); at locations where the preindustrial Greenland elevation is below 1300 m, we set LIG orography to zero meters, but define the ground to be ice covered and keep the albedo at values typical for the GIS (Fig. 1c); (3) a GIS similar to simulation LIG-1300m, but with albedo adjustment at locations where prescribed LIG orography is zero meters (LIG-1300m-alb); at such locations the land surface is defined as being ice-free and the background albedo is reduced from 0.7 to 0.16 (Fig. 1d), an albedo value that is typical for tundra (Fitzjarrald and Moore, 1992; Eugster et al., 2000) – this simulation, in combination with simulations LIG-1300m and LIG-ctl, allows us to separate the climatic effects of a lowered and spatially reduced GIS from those of changes in albedo; (4) a simulation similar to (3), but with an atmospheric concentration of CH_4 that is increased to 760 ppbv (LIG-1300m-alb-CH_4, Fig. 1d); this simulation enables us to quantify the combined effect of a lowered GIS elevation, changes in albedo and insolation with respect to PI.

Such changes in GIS elevation and extent would lead to a sea level rise of about 3 m instead of 7 m for the present situation due to the rebound effect (relaxation of the lithosphere). A sea level change of +3 m is in agreement with other studies that suggest an increase in sea level of 0.3 to 5.5 m during the LIG as a result of GIS melting (Cuffey and Marshall, 2000; Tarasov and Peltier, 2003; Lhomme et al., 2005; Otto-Bliesner et al., 2006; Carlson et al., 2008; Colville et al., 2011; Quiquet et al., 2013; Stone et al., 2013). Generally, other boundary conditions of the simulations are kept at their preindustrial state, except for vegetation which is computed dynamically according to the prevailing climate conditions (the only equilibrium simulation that considers fixed preindustrial vegetation is LIG-GHG).

Furthermore, we perform one transient model simulation that covers the Holocene (8–0 kyr BP) and four transient simulations of the LIG (130–115 kyr BP). The Holocene transient simulation is included in this study as a control run for the LIG transient simulations, in order to assess the differences and similarities between the present and last interglacial. For the LIG, we apply orography configurations of simulations LIG-ctl, LIG-×0.5, LIG-1300m-alb, and LIG-GHG, respectively. These LIG transient

simulations enable us to extract the temperatures at the LIG thermal maximum. The transient simulations are started from a near-equilibrium state, meaning that the climate system is already adjusted to the prescribed forcings, except for the ocean which needs about 3000 years in order to reach an equilibrium state. Performing such long equilibrium simulations is not feasible due to the involved computational effort. Each transient simulation is accelerated by a factor of ten in order to reduce the computational expense. To this end, astronomical forcing is accelerated following the method of Lorenz and Lohmann (2004). The astronomical parameters are calculated after Berger (1978). During the simulations, the trace gas concentrations remain fixed – except for the LIG-GHG-tr run, where a timeseries is prescribed according to Lüthi et al. (2008) for CO_2, Loulergue et al. (2008) for CH_4, and Spahni et al. (2005) for N_2O, as proposed for PMIP3. The respective values are interpolated to a 0.01 kyr resolution that corresponds to the accelerated model time axis. A fixed preindustrial vegetation is considered only in the LIG-GHG-tr simulation, in the other transient simulations vegetation is computed dynamically. For the Holocene run, the orography is identical to preindustrial conditions.

In order to determine whether TS anomalies between simulations are statistically significant or rather caused by internal variability (noise), we perform an independent two-tailed Student's *t* test *t* following Eq. (1). For each grid cell, it relates time averages X and standard deviations σ of model output time series of two given model simulations X_1 and X_2 of a length of n timesteps, in dependence of the effective degrees of freedom (DOF_{eff}). The DOF_{eff} are calculated considering the lag-1 autocorrelation acf (von Storch and Zwiers, 1999):

$$DOF_{eff} = n(1-acf)/(1+acf) \quad \text{with} \quad acf = \max(acf, 0),$$

meaning that the DOF_{eff} cannot be higher than 50, as the last 50 model years of each simulation are used for the analysis. For each grid point from X_1 and X_2 simulations, the smaller DOF_{eff} value is used for calculating the significance value with a 95% confidence interval.

$$t = \frac{\overline{X_1} - \overline{X_2}}{\sqrt{\frac{\sigma^2(X_1)}{n} + \frac{\sigma^2(X_2)}{n}}} \qquad (1)$$

Surface temperature at locations where the *t* test *t* of two data sets indicates a significance value below the critical value is considered to be statistically insignificant and is marked by hatches on geographical maps presented throughout this study.

For the analysis of time slice simulations, we define winter and summer as the mean of the 50 coldest and warmest months, respectively, for each grid cell, as we are mainly interested in local

seasons.In all performed simulations, a modern calendar is assumed. Although in reality the definition of seasons changes over time due to orbital precession, taking this calendar shift into account would only have a minor influence on our results since we calculate the summer and winter seasons by extracting the warmest and coldest month, respectively. Maximum and minimum LIG TS are calculated from the transient simulations considering the time interval between 130 and 120 kyr BP. In order to filter out internal variability, a 100-point running average representing the average over 1000 calendar years is applied. Maximum and minimum LIG warmth of the summer are defined as the warmest and coldest average of 100 warmest months, respectively, which reflects the warmest or coldest 1000 summer seasons with respect to the astronomical forcing. For the maximum and minimum LIG warmth of annual mean, we consider the warmest and coldest average of 100 model years, respectively. The seasonality range is defined by calculating the summer maximum LIG warmth (warmest average of 100 warmest months of the model years) and winter minimum LIG TS (coldest average of 100 coldest months of the model years).

2.3 Temperature reconstructions

In order to test the robustness of our simulations, we additionally perform a model-data comparison using proxy-based temperature anomalies that are available for the northern high latitudes (CAPE Last Interglacial Project Members, 2006), across the globe (Turney and Jones, 2010), and in the northern and southern middle to high latitudes (Capron et al., 2014). The temperature reconstructions from CAPE Last Interglacial Project Members (2006) are based on terrestrial and marine proxy records and estimate summer temperatures for maximum LIG warmth relative to PI. The global dataset by Turney and Jones (2010) comprises terrestrial and marine proxy records and estimates annual mean temperatures for maximum LIG warmth (terrestrial) and for the period of plateaued $\delta^{18}O$ (marine), relative to present day (PD, 1961–1990; Smith and Reynolds, 1998; New et al., 1999). The dataset by Capron et al. (2014) used in our study comprises marine- and ice core-based temperature reconstructions at the 130 and 125 kyr BP, as well as covering the LIG (125–115 kyr BP). This temperature compilation is the first one to comprise temperature reconstructions associated with a coherent temporal framework built between the ice core and marine sediment records (Capron et al., 2014). Detailed information regarding the proxy data is given in CAPE Last Interglacial Project Members (2006), Turney and Jones (2010), and Capron et al. (2014), respectively.

In order to quantify the agreement between model and data, we calculate the root-mean-square deviation (RMSD) which is a measure of the differences between an estimator (y_{model}) and estimated

parameter (y_{data}) (Gauss and Stewart, 1995; Mudelsee, 2010). RMSD is defined in Eq. (2):

$$\mathrm{RMSD}=\sqrt{\frac{1}{n}\sum_{i=1}^{n}\left(y_{\mathrm{model}}-y_{\mathrm{data}}\right)^2} \quad (2)$$

where y_{model} is the simulated TS anomaly at the location of the proxy record, y_{data} indicates the reconstructed TS anomaly, and n is the number of data samples.

3. Results

In the first part of this section, we present results from our LIG GIS sensitivity simulations, focusing on TS anomalies. Afterwards, a short description of results from the transient simulations is presented, followed by the model-data comparison and consideration of potential uncertainties in the model and data.

3.1 Greenland Ice Sheet elevation and albedo influence on global surface temperature

3.1.1 Annual mean anomalies

We first focus on annual mean TS anomalies. Figure 2 presents the effect on the global TS of lowering the GIS by half its preindustrial elevation by various methods. We observe the strongest warming over Greenland (of up to +12.5°C) in the simulation with a reduction in GIS of 1300 m and albedo changes wherever the land surface is changed from ice-covered to tundra (LIG-1300m-alb, Figs. 1c and 2c). When reducing GIS by half its preindustrial elevation applying the first method described in Data and Methods section (LIG-×0.5 simulation, Figs. 1a and 2a), Greenland warms by up to +11.1°C. Northern North America and the Arctic Ocean warm by up to +2°C in all GIS sensitivity simulations. The most widespread warming is simulated in LIG-×0.5 (Fig. 2a), while the LIG-1300m-alb simulation presents a less widespread warming but a higher increase in TS over the Arctic Ocean, where anomalies of +2°C are simulated (Fig. 2c). A pronounced warming is found over the southernmost Southern Ocean of up to +4°C (Fig. 2a–c).

The highest global mean TS anomaly is simulated in LIG-1300m-alb simulation with an average of ΔTS = +0.37°C, though is higher by only +0.01°C than the average derived from LIG-×0.5 simulation, and by +0.07°C than LIG-1300m simulation. Changes in GIS configuration lead to strongest anomalies in the Northern Hemisphere, with average TS changes of ΔTS = +0.47°C in LIG-×0.5 simulation, ΔTS = +0.38°C in LIG-1300m, and ΔTS = +0.43°C in LIG-1300m-alb simulation. The highest average TS

changes in the Southern Hemisphere are simulated in LIG-1300m-alb with ΔTS = +0.31°C, while in LIG-1300m and LIG-×0.5 simulations the average TS anomalies are ΔTS = +0.20°C and ΔTS = +0.24°C, respectively. Consequently, the exact method of changing GIS configuration influences the hemispheric temperature anomalies.

The most affected areas by changes in GIS configuration are the northern high latitudes, which experience a warming of ΔTS = +1.45°C in LIG-1300m-alb simulation, and ΔTS = +1.07°C and ΔTS = +1.03°C in LIG-×0.5 and LIG-1300m simulations, respectively. This indicates that albedo plays a significant role in the northern high latitude temperature changes, causing an average temperature anomaly of ΔTS = +0.42°C. A local cooling of up to −1.60°C is limited to the Barents Sea in LIG-×0.5 and LIG-1300m simulations (Fig. 2a, b), south-west of Greenland in LIG-1300m simulation (Fig. 2b), and a cooling of up to −2.30°C over the Sea of Okhotsk (western Pacific Ocean) in LIG-1300m-alb simulation caused by a reduction in albedo in the prescribed ice-free areas (Fig. 2c, d). In the latter simulation, the Barents Sea cooling is counteracted by a warming caused by changes in albedo (Fig. 2d).

At 130 kyr BP, the AMOC was reduced by 3.5 Sv as compared to the PI (Table 2). However, a reduction in GIS partly counteracts the negative anomaly and leads to an increase in the AMOC of up to 2.2 Sv relative to the control simulation LIG-ctl. The applied method of changing GIS configuration has an influence also on the simulated changes in AMOC. In the LIG-×0.5 simulation, there is rather a minor increase in AMOC of 0.5 Sv, while in LIG-1300m simulation AMOC is increased by 2 Sv. In the LIG-1300m-alb, AMOC is enhanced by 2.2 Sv, meaning that changes in albedo further contribute an increase of 0.2 Sv (Table 2).

3.1.2 Winter and summer mean anomalies

The seasonal effect of a reduced GIS elevation is strongest during local winter in both hemispheres in all GIS sensitivity simulations(Table 2). However, for simplicity we focus here only on the GIS sensitivity simulation that includes changes in GIS elevation and corresponding changes in albedo (LIG-1300m-alb, Fig. 3). The TS anomalies between the LIG control simulation LIG-ctl and the other two GIS sensitivity simulations (LIG-×0.5 and LIG-1300m) can be calculated from the TS averages given in Table 2. In the Northern Hemisphere, winter TS changes by ΔTS = +0.57°C. The corresponding change in the Southern Hemisphere winter is ΔTS = +0.39°C and the global average is ΔTS = +0.48°C (Fig. 3a). The changes in GIS elevation and albedo lead to a winter warming of ΔTS = +2.08°C in the northern high latitudes.

During summer, the TS anomaly is also positive but of lower magnitude, with an average of ΔTS = +0.24°C for Northern Hemisphere, Southern Hemisphere, and globally (Fig. 3b). The northern high latitudes warm during summer by ΔTS = +0.46°C, which is a modest change compared to winter warming. Relatively strong cooling occurs over the Sea of Okhotsk and south-west of Greenland (Fig. 3), again with the strongest effect being present during winter. The sea ice edge and 50 %-compactness isolines are subject to local poleward retreat in the case of changed GIS and albedo.

3.2 Combined effects of LIG forcings on global surface temperature

The combined effects on TS of reducing the GIS by 1300 m, adjusting albedo, and applying astronomical changes that represent an LIG climatic setting are presented in Fig. 4. Assuming linearity of the different climatic drivers, we can additionally split the anomaly of simulations PI and LIG-1300m-alb-CH_4 (equivalent to simulation LIG-1300m-alb, but with a CH_4 concentration adjusted to PI simulation) into the isolated contributions of changes in elevation and albedo and in astronomical forcing. The anomaly caused by the astronomical forcing is calculated as the difference between the anomaly of LIG-1300m-alb-CH_4 and PI, and the anomaly of LIG-1300m-alb and LIG-ctl. Considering Table 2, we find that the magnitude of the astronomical forcing influence is stronger than the effects of lowering the GIS and respective adjustment of the albedo in the global average of annual mean TS, as well as the annual mean average over Northern Hemisphere (Fig. 4a). In the Southern Hemisphere, both forcings have equal contributions to changes in annual mean TS (Fig. 4a). During winter, changes in GIS have the strongest influence globally and in the Northern Hemisphere, while in the Southern Hemisphere changes in astronomical forcing are dominant (Fig. 4b). During summer, there is an opposite pattern. Insolation changes are dominant globally and in the Northern Hemisphere, while the Southern Hemisphere is mostly influenced by changes in GIS and albedo (Fig. 4c). The strongest combined effect of insolation and changes in GIS and albedo occurs in the Northern Hemisphere during summer with an anomaly of ΔTS = +2.51°C. Globally, the combined effect leads to a warming of ΔTS = +1.34°C during summer. In the Southern Hemisphere, the strongest combined effect is simulated during winter with ΔTS = +1.08°C. The highest annual mean average TS anomaly due to the combined forcing is found over Greenland with up to ΔTS = +13.9°C, while the strongest cooling caused by insolation is located over central Africa, the Arabian Peninsula, and India (locally ΔTS = −5.3°C, Fig. 4a).

The winter (local minimum TS) of the LIG is in general cooler than the PI at northern low to middle latitudes, while at northern high latitudes and Southern Hemisphere winter is warmer (Fig. 4b).

If we separate the astronomical effect from the GIS lowering and albedo changes, we can attribute to insolation a cooling of ΔTS = −0.52°C in Northern Hemisphere, and a warming of ΔTS = +0.69°C in Southern Hemisphere. Due to warmer high latitudes, the sea ice edge and 50 % sea ice compactness isolines are located closer to the continents in LIG relative to PI (Fig. 4b).

Summer (local maximum TS) anomalies of the LIG with respect to PI are stronger than winter anomalies in the Northern Hemisphere (Fig. 4c). Strongest continental summer TS anomalies are located in the Northern Hemisphere (up to ΔTS = +16.7°C). Locations where the LIG is cooler than PI are found at ∼10°N over Africa and at ∼25°N over India. Figure 4c also depicts the locations of the sea ice edge and the 50 % sea ice compactness isolines, which indicate that, in the Arctic Ocean, LIG summer sea ice is more strongly reduced compared to PI than winter sea ice. The summer LIG Arctic Ocean sea ice cover does not exceed 50 %-compactness anywhere. In the Southern Ocean there is no such clear seasonal bias.

3.3 Surface temperature evolution during the present and Last Interglacial

In Figs. 5, S2, and S3, a comparison of transient TS derived from the five transient simulations (Table 1) is shown. The LIG transient simulations are important for determining when the maximum LIG warmth occurred in dependence of the location as well as seasons. For simplicity, we display here only the TS evolution in the northern high latitudes (60–90°N, Fig. 5). All LIG (130–115 kyr BP) simulations (LIG-ctl-tr, LIG-×0.5-tr, LIG-1300m-alb-tr, and LIG-GHG-tr) indicate a similar annual mean trend, starting with a plateau until mid-LIG (around 123 kyr BP) . After mid-LIG, there is a pronounced cooling trend in all LIG transient simulations (Fig. 5a). The control simulation LIG-ctl-tr starts at a slightly higher TS than the LIG-GHG-tr, but although the trace gas concentrations are mostly lower throughout the latter, the LIG-GHG-tr simulates higher TS throughout the LIG. This indicates that changes in the vegetation which are simulated in the LIG-ctl simulation lead to a cooling in the Northern Hemisphere, partly counteracting the warming induced by higher GHG concentrations. Even warmer TS are observed in the LIG-×0.5-tr, due to the changes in GIS elevation. The most extreme case is represented by the simulation LIG-1300m-alb-tr, which shows predominantly the highest TS relative to TS of other LIG transient simulations. When calculating the linear TS trends over 15 kyr covering the LIG (130–115 kyr BP), simulation LIG-×0.5-tr presents the steepest trend with a value of −3.97°C. LIG-GHG-tr represents the weakest trend, namely −2.95°C. The Holocene (8–0 kyr BP) transient simulation (HOL-tr) starts also with a warming (+1.45°C) until around mid-Holocene (6 kyr BP), followed by a cooling trend. The trend over the last 8 kyr is negative, with a value of −1.76°C.

During winter, all LIG simulations indicate a positive trend in the early LIG, with maximum TS at around mid-LIG (Fig. 5b), followed by a strong cooling. The relative order of magnitudes of TS trends during different simulations is the same as for annual mean TS, but with a relatively larger offset in between simulations. The strongest winter TS trend during the LIG is present in simulation LIG-×0.5-tr, with a cooling of −2.47°C. The smallest trend is simulated in LIG-GHG-tr simulation, namely −1.08°C. Simulation HOL-tr shows a warming of +0.8°C, followed by a cooling trend that starts at mid-Holocene (Fig. 5b). Overall, the Holocene TS trend is −1.73°C. Winter TS are characterized by stronger temporal variability than summer TS (Fig. 5b, c). Summer TS in all LIG simulations indicate a slight warming trend until around 128 to 126 kyr BP, followed by a pronounced cooling. The strongest trend during summer is present in simulation LIG-ctl-tr (−6.26°C), while the smallest is derived from LIG-GHG-tr simulation (−5.94°C). The offset between transient TS is smaller than for annual mean and winter, but with the same order on the temperature scale. A dramatic cooling is also present in the Holocene simulation, which shows a trend of −2.28°C starting at mid-Holocene (Fig. 5c). Furthermore, the timing of the maximum LIG warmth does not occur simultaneously between the winter and summer seasons, the winter season indicating a later peak than summer (Figs. 5, S2, and S3).

3.4 Comparison of model results to temperature reconstructions

Due to the large amount of simulated data, we display in the model-data comparison simulated LIG TS derived from only one equilibrium simulation with changes in GIS, namely LIG-1300m-alb. For the calculation of the maximum LIG warmth, we consider the corresponding LIG-1300m-alb-tr transient simulation. However, the comparison of the proxy-based temperatures with the other GIS sensitivity simulations is considered in Table S1 in the Supplementary material, which gives the RMSD values between temperature reconstructions and simulated TS extracted at the location of each given proxy record and derived from simulations with different GIS boundary conditions. Furthermore, we display also results from LIG-ctl equilibrium simulation for 130 kyr BP and LIG-ctl-tr transient simulation for maximum LIG warmth, in order to determine if and where GIS changes lead to an increase in model-data agreement.

3.4.1 Proxy-based summer temperature reconstructions

Figures 6, 8a, and S4a present a model-data comparison that consider LIG terrestrial and marine proxy-based summer temperature anomalies relative to PI derived by CAPE Last Interglacial Project Members (2006). Simulated and reconstructed temperature anomalies agree reasonably well with respect to the sign of the change, in the simulation with a reduction in GIS (Fig. 6a) and with

preindustrial GIS configuration (Fig. 6c). The best agreement between model and proxy reconstructions occurs over northern Asia and Europe. In the North Atlantic Ocean and the Arctic Ocean, the model underestimates marine-based temperature reconstructions (Fig. 6a, c). There is nearly no TS change present in the model, while the marine records indicate anomalies of +1 to +4°C. However, a reduction in GIS and albedo leads to slightly higher summer temperature anomalies at the location of some marine proxies in the North Atlantic Ocean, partly reducing the model-data mismatch (Fig. 6a).

Over Greenland, the elevation changes lead to an overestimation of the reconstructed temperature anomalies – proxy records show anomalies of +4 to +5°C, while the simulated TS anomalies are above +7°C (Fig. 6a). In the control simulation, LIG-ctl, there is an underestimation of the reconstructed temperatures (Fig. 6c). An overestimation of the proxy reconstruction by the model is present over Alaska, where the simulated TS changes in the LIG-1300m-alb simulation are within +3 to +4°C, while the terrestrial proxy-based temperature anomalies are between +0 and +2°C. However, in the LIG-ctl simulation, the differences between model and data are smaller.

In addition to the 130 kyr BP LIG simulation (LIG-1300m-alb), for each given core location we also consider TS anomalies relative to PI calculated at the minimum and maximum LIG summer warmth as derived from the transient simulation LIG-1300m-alb-tr (Fig. 8a). In the case of the terrestrial proxies, the temperature span covers +2 to +6°C, but 0 to +10°C (Fig. 8a) if we consider the uncertainty temperature intervals from which we chose the values closest to corresponding model results. The respective simulated anomalies cover +1 to +11°C, the largest anomalies being located over Greenland (Fig. 6a). When we consider also the simulated TS anomalies at the summer minimum and summer maximum LIG warmth for each record, in about half the cases (14 records out of 27) the error bars touch the 1 : 1 line, possibly indicating better agreement than when compared to LIG TS anomalies at 130 kyr BP (Fig. 8a). The number of 13 unresolved records can be reduced to 11, when the terrestrial proxy-based temperature anomalies are compared to the simulated TS anomalies that are derived from the simulation with PI GIS elevation (LIG-ctl-tr, Fig. S4a). Marine-based temperature anomalies and the corresponding simulated anomalies (from LIG-1300m-alb) are of lower magnitude than their terrestrial counterparts, with a marine-based temperature anomaly span of 0 to +3°C (and 0 to +4°C temperature uncertainty) and simulated TS anomaly span of ~0 to +4°C (Fig. 8a). Only one marine record, located on the eastern coast of Greenland, shows an underestimation of at least 6°C (Fig. 6). Seven out of thirteen marine records cannot be reconciled with the simulations when considering maximum and minimum summer TS anomalies during the LIG (Fig. 8a). The LIG-ctl-tr simulation as

well can resolve only 6 records (Fig. 6d and S4a). When the reconstructed data is compared to simulated annual mean TS anomalies at 130 kyr BP (Figs. S5a, c and S6), we find an even higher discrepancy than when compared to the summer average, implying that the reconstructed records are indeed biased towards summer. Furthermore, there are 20 terrestrial and 8 marine records that cannot be resolved by using annual mean minimum or maximum LIG warmth in the LIG-1300m-alb-tr (Figs. S5b and S6a), and 21 terrestrial and 8 marine records in the LIG-ctl-tr (Figs. S5d and S6b).

The proxy dataset by CAPE Last Interglacial Project Members (2006) is considered to represent summer temperatures at the maximum LIG warmth. Thus, we additionally include in the model-data comparison the simulated maximum LIG warmth calculated from our transient LIG simulations (Fig. 6b, d). We find that the agreement between model and data increases in some cases. Over northern Asia, for example, highest simulated summer TS anomalies occur between 126.5 and 129.5 kyr BP (Fig. 9a), and are in better agreement with the proxy records than when simulated anomalies at 130 kyr BP are considered. For the northern North Atlantic Ocean, marine records agree best with simulated TS anomalies at the maximum LIG warmth (between 121.5 and 124.5 kyr BP, Fig. 9a) in the LIG-1300m-alb simulation (Fig. 6b). However, the RMSD between the simulated TS and reconstructed temperature anomalies reveals that the best agreement occurs with TS anomalies at maximum LIG warmth in the LIG-ctl-tr simulation (Table S1 in Supplementary material). A reduction in GIS, thus, does not improve in general the model-data agreement when the dataset by CAPE Last Interglacial Project Members (2006) is considered. However, changes in GIS lead to high temperature anomalies during local winter (Fig. 3a), while summer season is not strongly influenced (Fig. 3b). Therefore, in a comparison with proxy reconstructions that represent summer temperature anomalies, changes in GIS do not have a significant impact on model-data agreement.

3.4.2 Proxy-based annual mean temperature reconstructions

Both reconstructed and simulated global annual mean temperature anomalies (Fig. 7) indicate that the high latitudes experienced warmer temperatures during the LIG than in the PI, with strongest anomalies being present in the northern high latitudes. However, the model underestimates the strong positive anomalies derived from proxy records, and in low and middle latitudes the model cannot capture the magnitude of the cooling that the proxy records show (Figs. 7a, c, 8b, and S4b).

Changes in GIS have no significant influence in low to middle latitudes but cause strong positive anomalies in the northern high latitudes thus improving the model-data comparison (Fig. 7a, Table S2), although the model still underestimates the proxy reconstructions. Terrestrial proxy records indicate

stronger anomalies with ΔTS = +2.21°C (globally), ΔTS = +2.21°C (Northern Hemisphere), and ΔTS = +2.11°C (Southern Hemisphere). Consideration of the simulated anomalies at locations of terrestrial records indicates a global average of ΔTS = +1.44°C, underestimating the records by ∼1°C. The Northern Hemisphere and Southern Hemisphere average TS anomalies are ΔTS = +1.48°C and ΔTS = +0.92°C, respectively. Marine records capture lower anomalies than their terrestrial counterparts but still larger anomalies than the corresponding simulated anomalies.

The majority of the terrestrial records shows a stronger signal than the simulated anomalies (Fig. 8b). The temperature anomaly range in the terrestrial reconstructed data covers −5 to +15°C, while the model covers 0 to +12°C. The proxy records that indicate the most extreme negative temperature anomalies (31 records out of 100) are not fully reconciled with simulations by considering the minimum LIG values derived from the model. For positive temperature anomalies, there are 36 records that agree better with the model simulation when the maximum LIG warmth is considered, but the error bars do no touch the 1 : 1 line indicating as well a persistent deviation (Fig. 4b). The remaining 33 terrestrial records agree with the model data somewhere between the annual mean minimum and maximum LIG warmth. This is a slightly better result than for simulation LIG-ctl-tr, in which case only 19 terrestrial records can be resolved by considering minimum and maximum TS intervals (derived from LIG-ctl-tr, Fig S4b). When we consider marine proxy-based temperature anomalies, the model-data agreement is lower than in the case of their terrestrial counterparts. The reconstructed marine temperature anomalies cover a range of −6 to +11°C compared to 0 to +3°C in the model, indicating pronounced underestimation of the marine proxy-based anomalies by the model. Low temperature anomalies are mostly located at low latitudes, where the magnitude of temperature change is higher in the reconstruction than in the model (Figs. 7a and 8b). When we consider both annual mean minimum and maximum LIG warmth, the simulated TS span increases by ∼1°C (−0.5 to +3.5°C). Considering the annual mean maximum LIG warmth, 71 (out of 162) marine records that show positive anomalies cannot be reconciled with the simulation. From the records that show negative anomalies, 71 cannot be resolved by TS anomalies at minimum LIG. The remaining 20 records agree with the model data between the minimum and maximum LIG warmth with respect to annual mean. The marine records are slightly better reconciled when LIG-ctl-tr is considered, with 25 records being reconciled with the simulation by the minimum and maximum LIG warmth (LIG-ctl-tr, Fig. S4b).

The proxy records derived by Turney and Jones (2010) are considered to record an annual mean temperature signal. Nevertheless, some records may be biased towards a specific season. Therefore, we

also consider the minimum winter and maximum summer TS during the LIG (Fig. 4c). Seasonality increases the span of the vertical bars, providing the possibility of a better agreement with the reconstructed temperature anomalies. The agreement between proxy records and model simulations increases, with 51 terrestrial and 53 marine records being reconciled by considering seasonality (Fig. 4c). An even better agreement is found when the terrestrial proxy-based temperature anomalies are compared to the simulated seasonality range derived from simulation LIG-ctl-tr. In this case, for 69 terrestrial records the vertical bars touch the 1 : 1 line (Fig. 4c). For the marine proxies a number of 51 records can be reconciled with the simulation by considering seasonality as derived from simulation LIG-ctl-tr.

As already mentioned, the terrestrial proxy records by Turney and Jones (2010) are considered to record annual mean temperature anomalies at the maximum LIG warmth. Therefore, we additionally compare the terrestrial records with the simulated annual mean at the LIG thermal maximum (Fig. 7b, d). Over Europe, the agreement between model and data is increased for those records that indicate a warming, as the modelled anomalies derived from LIG-1300m-alb-tr simulation indicate a warming at the maximum LIG warmth, while presenting nearly no change at 130 kyr BP (Fig. 7a). Over northern Europe, maximum LIG warmth occurs at mid-LIG between 122.5 and 123.5 kyr BP (Fig. 9b). There is a slightly better agreement for the records located in northern Asia. At these locations, the highest TS anomalies are found towards the first part of the LIG (between 126.5 and 129.5 kyr BP). According to Table S2 in the Supplementary material, the terrestrial proxy-based temperature anomalies indicate the best agreement with the simulated annual mean TS at the maximum LIG warmth derived from the LIG-1300m-alb simulation. The annual mean anomalies are influenced by winter temperatures, the season during which GIS leads to strong positive anomalies. Therefore, a model-data comparison with proxy reconstructions that represent an annual mean signal shows a better agreement than when summer proxies are considered.

3.4.2 Time resolved proxy-based summer temperature reconstructions

For a more robust model-data comparison, we additionally compare our simulated TS to a compilation of high-latitude LIG temperature anomalies derived from synchronized records representing 130 kyr BP (Figs. 10 and S12, Capron et al., 2014). The synchronization is performed by aligning marine sediment records onto the recent AICC2012 ice chronology (Capron et al., 2014 and references therein). This method reduces the uncertainty in relative dating of the proxy reconstructions. The temperature reconstructions are mostly located in the North Atlantic Ocean and Southern Ocean. The

marine records from the North Atlantic Ocean indicate mostly negative anomalies, while the model simulates nearly no changes. As shown above, GIS reduction leads to a small increase in summer TS anomalies, thus increasing the model-data disagreement (Figs. 10a and S12a). A warming in the Southern Ocean is captured by both the model and proxies, though the model underestimates the reconstructions. Reducing the GIS and albedo leads to an increase in local summer TS anomalies in the Southern Ocean bringing the model and data in slightly closer agreement (Figs. 10b and S12b).

Considering Table S3 in Supplementary material, the reconstructed temperatures agree best with the simulated summer TS at 125 kyr BP in simulation LIG-125k (Fig. S15) which considers a reduced GIS configuration (as in the LIG-1300m-alb simulation), both indicating a warming. However, this result is not conclusive with respect to the GIS elevation, as a simulation with preindustrial GIS elevation has not been yet performed for this particular time slice. For 130 kyr BP, the best agreement occurs for the LIG-ctl simulation but for annual mean rather than summer; since the model simulates an annual mean cooling in the North Atlantic Ocean (Fig. S5c).

The proxy record compilation is used in the model-data comparison by Capron et al. (2014), using two different climate models, namely CCSM3 and HadCM3. For 130 kyr BP, a model-data mismatch is found in both cases, as most of the records indicate strong negative anomalies at 130 kyr BP, while the models simulate strong positive anomalies, especially CCSM3 which simulates higher GHG concentrations than HadCM3 and COSMOS. With respect to difference between model and data, COSMOS simulates TS closer to the temperatures derived from marine-based records, since it simulates nearly no change rather than a strong opposite signal. One cause for this modest change in the North Atlantic Ocean may be related to vegetation changes, which may lead to a cooling as suggested above. For 125 kyr BP, COSMOS simulates higher anomalies in the North Atlantic Ocean than at 130 kyr BP, but lower than CCSM3 and HadCM3 which simulate SSTs closer to the reconstructed temperatures. Note that the definition of summer is different in our study than in the study by Capron et al. (2014), as they calculate it as the average of July-August-September, while we consider the warmest month.

A model-data comparison of LIG temperature trends is also considered in our study (Figs. S13 and S14). The proxy-based temperature trends by Capron et al. (2014) is compared to the temperature evolution derived from our transient simulations (LIG-ctl-tr and LIG-1300m-alb-tr), between 125 and 115 kyr BP. An underestimation of the proxies by the model is again found, as well as an overestimation depending on the locations (Figs. S13 and S14). Changes in GIS do not strongly

influence the results, with the exception of a few locations where such changes lead to a less pronounced warming simulated in LIG-ctl-tr, thus reducing the mismatch.

4. Discussion

4.1 Effects of iInsolation and Greenland Ice Sheet elevation on surface temperature

The main focus of our study is to quantify the possible contribution of reduced GIS elevation in comparison with the contribution of insolation forcing to the climate of the LIG.

We can confirm the importance of insolation for the Northern Hemisphere, especially for the northern middle to high latitudes (Figs. 4, 6, 7, 10). The belt of decreased TS, observed around 10°N over Africa and 25°N over Arabian Peninsula and India (Figs. 4a, b and 7a), is related to increased cloud cover (Fig. S9) and increased summer precipitation of up to +6 mm d^{-1} (not shown). This effect has been described by Herold and Lohmann (2009), who propose a mechanism for the temperature anomalies that relies on changes in insolation in conjunction with increased cloud cover and increased evaporative cooling.

In general, and independent of GIS elevation we observe an annual mean global warming of ΔTS= +0.44°C in our LIG simulations relative to PI, hinting to positive feedbacks (such as sea ice-albedo) that amplify the high latitude insolation signal (Fig. 4).

In Section 3.1.2 we have shown that the most pronounced impact of reduced GIS elevation (in LIG-1300m-alb simulation) occurs during local winter in both hemispheres (Fig. 3a). The winter warming of up to +3°C over the Arctic Ocean may be linked to a decrease in sea ice and a delayed response to a warming occurring in October (not shown) which is caused by positive sea-ice-albedo feedbacks. A decrease in albedo over Greenland has the strongest influence during summer especially over the southernmost region (Figs. 2d and 3b), caused by insolation absorption by the ice-free land surface. Furthermore, we note cold annual mean anomalies in the Barents Sea (Fig. 2a, b) and Sea of Okhotsk (Fig. 2c) caused by an increase in sea ice cover... T

The change in the GIS elevation leads also to a relatively strong warming in the southern high latitudes, mainly off the coast of Antarctica, with the strongest positive anomaly occurring during local winter (Fig. 3a) that coincides with a heat flux transfer anomaly from the ocean to the atmosphere (not shown). Increased ocean heat flux during winter leads to a warming of the atmosphere. The Antarctic warming is most likely related to warmer deep water as well as subsurface warming poleward of 50°N

in the North and South Atlantic Ocean. The warming may be attributed to enhanced AMOC (Table 2), which plays an important role in the exchange of heat between the hemispheres and between atmosphere and ocean. Our results indicate a weaker AMOC during the LIG as compared to the PI of up to 3.5 Sv, but changes in GIS lead to an increase of up to 2.2 Sv. The simulated increase in AMOC in the sensitivity simulations may be triggered by increased salinity of up to + 1 psu in the northern North Atlantic Ocean. Increased salinity cannot be explained by changes in precipitation minus evaporation, which show positive anomalies in this area (not shown). Another contributing factor to the enhanced AMOC may be an increase in the atmospheric flow due to a reduction in GIS elevation. The low pressure system over Greenland and the high pressure system above Europe become more extreme, enhancing the north-eastward air circulation (Fig. 11). We find that the higher the sea level pressure (SLP) anomaly, the stronger the AMOC (Table 2, Fig. 11). This change could also explain the positive TS anomalies of up to +1°C in the northern North Atlantic Ocean, with more heat being transported poleward from the low latitudes (Fig. 2a–c). However, convection cannot be the only explanation for the southern high latitudes warmth, since the heat would be dispersed towards the Southern Hemisphere. We however note a large scale warming in the subsurface of the Southern Ocean which is probably caused by positive feedbacks. This warming may be related to changes in the water stratification. We observe an invigorated vertical mixing in the northern North Atlantic Ocean and a suppressed vertical mixing in the Southern Ocean (not shown), the latter causing the heat at subsurface to be preserved. The Southern Ocean has a large heat capacity leading to a long memory of the system. Lags of up the three months occur in the surface layer including sea ice (amplifying factor via positive ice-albedo and ice-insulation feedbacks), while long-term lags occur in deeper levels below the summer mixed layer that store seasonal thermal anomalies (Renssen et al., 2005).

In contrast to our results that show an increase in the AMOC relative to GIS elevation changes, Otto-Bliesner et al. (2006) and Bakker et al. (2012) find a weakening of the AMOC. Bakker et al. (2012) infer that the AMOC is weaker by up to 14 % in a regional study of LIG climate of the North Atlantic Ocean, prescribing a reduction of GIS elevation (by 700 m) and extent (reducing the ice volume by 30%). The weakening of the AMOC is caused by additional freshwater runoff resulting from a melting GIS, a factor that is not considered in our study and that would probably cancel out or reduce the effect of changes in the atmospheric transport on the AMOC. In the study by Bakker et al. (2012), reducing GIS elevation and extent leads to changes in the atmospheric flow pattern and creates a special pattern of surface pressure anomalies. In particular in the Norwegian Sea, Barents Sea, and

south-east of Greenland, the low pressure system is weaker inhibiting the overturning circulation.

The reduction of the GIS elevation and albedo alone leads in the study by Bakker et al. (2012) to a local warming of up to +4°C in July, a substantially lower anomaly (factor of ∼3) than simulated in our model for local summer when reducing both GIS and albedo. However, when comparing their simulated data to proxy-based temperature anomalies relative to PI (CAPE Last Interglacial Project Members, 2006), Bakker et al. (2012) find an overestimation of the temperature reconstruction over Greenland, and an underestimation at eastern Europe and Baffin Island – locations where we find a similar temperature tendency (Fig. 6a).

Another climate model study that considers a reduction in GIS topography by various methods has been performed by Merz et al. (2014). In their GIS sensitivity simulations, performed with the Community Climate System Model (version 4, CCSM4), they find a rather mixed signal in temperature anomalies over Greenland relative to the predominant warming found in our simulations with changes in GIS. During local winter, their model simulates a warming of up to +5°C in central Greenland and a cooling of up to -12°C in areas that become flat and ice-free. However, changes in topography of GIS do not have a significant influence on climate in the surrounding areas in the study by Merz et al. (2014). This may be caused by the fact that in their simulations SSTs are prescribed, while in our study the atmosphere model is interactively coupled to an ocean general circulation model. However, in their study the GIS is reconstructed by means of high resolution ice sheet models, while we consider a relatively simplistic representation of the GIS. Differences are found also with respect to changes in low-level winds. They find a rather local influence of the GIS changes and no major effect on the large-scale atmospheric circulation. Our model simulates an enhancement of low-level winds around GIS and on SLP (Fig. 11). As such, the methods of reducing GIS and the model used have a strong influence on the local and large-scale climate. Note, however, that the aims of our study and the study by Merz et al. (2014) are different, since the latter focuses on local effects above Greenland, while our main focus is on the GIS effects on large-scale climate.

4.2 Surface temperature evolution during the Last Interglacial and the Holocene

Although our results are not directly comparable to those derived by Bakker et al. (2013), who analyze transient LIG January and July temperature anomalies (simulated by seven different models) with respect to PI while we use transient absolute TS for coldest and warmest month, the pattern of the temperature evolution remains the same. We observe similarities in middle latitudes and in winter

temperatures at high latitudes characterized by a large variability, and also note a clear cooling trend for summer caused by a decrease in summer insolation. At northern high latitudes, Bakker et al. (2013) find July maximum LIG warmth at 128.4–125.1 kyr BP, while in middle latitudes the maximum occurs at 129.4–126.3 kyr BP. We also observe a warmest month maximum at around 128 kyr BP for high and middle latitudes. A July maximum LIG warmth is found in the study by Loutre et al. (2014) at 128 kyr BP. They find that the summer SST during the LIG is smaller in the model than in the reconstructed temperatures, especially in the North Atlantic Ocean, but taking into account the evolution of the Northern Hemisphere ice sheets reduces the disagreement between model and data.

During winter, our simulations produce a clear high latitude TS maximum around mid-LIG, while the middle latitudes experience peak warmth around 121–117 kyr BP. Bakker et al. (2014) compare transient LIG and Holocene (8–0 kyr BP) temperature trends simulated by different models (including our COSMOS LIG-GHG-tr and HOL-tr simulations). They find negative warmest month temperature trends for both LIG and Holocene in the Northern Hemisphere, and they propose that the climate reacts linearly to changes in insolation. Bakker et al. (2013) find a linear relation between changes in insolation and temperatures for both summer and winter and for all latitudes. There are however some exceptions. In northern high-latitudes, the winter temperature changes result mainly from sea-ice related feedbacks and are described as highly model-dependent. In southern middle to high latitudes, winter temperatures are strongly affected by changes in GHG concentrations. Comparing all LIG transient simulations with the Holocene in the three considered latitudinal bands, we observe that the Holocene experiences mostly lower TS than during the LIG, and is characterized by smaller trends.

In our LIG transient simulations, we find that the differences in TS between the different model simulations at the beginning of the LIG (130 kyr BP) are higher than during the late LIG (115 kyr BP), indicating that the impact of a reduced GIS is stronger at the beginning of the LIG as compared to glacial inception (GI, 115 kyr BP). By using different approaches to simulate the LIG evolution, we offer a bandwidth of possible temperatures at each given time.

4.3 Model-data comparison

In combination with changes in the GIS elevation and lower albedo, the insolation effect causes strong positive TS anomalies in the Northern Hemisphere, especially during summer (Figs. 4c and 6a). The pattern of these changes is observed also in a model study of the LIG that includes changes in GIS elevation of 500 m (Otto-Bliesner et al., 2006). The study shows that the June-July-August (JJA) temperature anomaly with respect to PI is positive in the Northern Hemisphere especially over the

continents – yet, the magnitude of these changes is smaller than in our study. The Barents Sea experiences no temperature change in Otto-Bliesner et al. (2006), compared to a warming of +2 to +4°C simulated by our model. The only location in simulations by Otto-Bliesner et al. (2006) that is notably warmer than in our simulations is at the western side of Greenland – the high decrease in GIS elevation prescribed in our simulation is accompanied by modest TS anomalies at the western side of Greenland, which may be related to an increase in the sea ice. In order to validate their results, Otto-Bliesner et al. (2006) compare the simulated temperature anomalies to proxy-based temperature anomalies by CAPE Last Interglacial Project Members (2006), the same temperature reconstruction data that we use in our model-data comparison (Figs. 6, 8a, S4a, S5, S6, and S10). Comparing our model results with the marine and terrestrial reconstruction temperatures by CAPE Last Interglacial Project Members (2006), we see most similarities with respect to temperature in the summer anomalies of LIG relative to PI, although at some locations the magnitude differs. At the western side of Greenland, our model underestimates the terrestrial proxy-based temperature anomalies by at least 2°C, while in Alaska there is an overestimation, making the model-data agreement of Otto-Bliesner et al. (2006) better. Over Greenland, the warming reaches +5°C according to the proxy reconstructions, while our results show a higher warming caused by the reduction of the GIS.

Over Greenland, the model overestimates the proxy-based temperature anomalies, while the results from Otto-Bliesner et al. (2006) indicate an underestimation. This suggests that the GIS elevation during the LIG may have not been so drastically reduced as prescribed in our model setup, but was still reduced by at least 500 m. This conclusion is supported also by another study (Stone et al., 2013) that compares simulated LIG TS anomalies relative to PI to anomalies derived from the reconstruction by CAPE Last Interglacial Project Members (2006). In their simulation, which was produced using the coupled atmosphere–ocean general circulation model HadCM3 (Hadley Centre Coupled Model, version 3), Stone et al. (2013) find a good agreement between model and reconstruction as well, but cannot capture the reconstructed strong warming over Greenland, their simulation indicating a warming of up to +3.5°C. They imply that the GIS was reduced in the LIG as compared to PI, but not completely deglaciated – in the simulation with a completely removed GIS, they find much stronger temperature anomalies over Greenland of up to +16°C, higher than in our findings when GIS is reduced to half its present elevation (Fig. 2).

Proxy records based on ice cores indicate over Greenland positive summer anomalies of up to +5°C at the maximum LIG warmth (Johnsen et al., 2001; NGRIP members, 2004). The corresponding

simulated temperature anomalies at Renland ice core site (Johnsen et al., 2001) are +4.93°C in the LIG-ctl simulation and +8.71°C in the LIG-1300m-alb simulation, indicating that in eastern Greenland, the height of the ice sheet was probably similar to preindustrial elevation. An overestimation by the model occurs at NGRIP ice core location (NGRIP members, 2004), whether changes in GIS are taken into account or not, the LIG-ctl and LIG-1300m-alb simulations indicating a warming of +7.46°C and of +11.13°C, respectively. A warming as high as +8 ± 4°C is proposed by Dahl-Jensen et al. (2013) for the peak LIG warmth at 126 kyr BP, based on North Greenland Eemian Ice Drilling (NEEM) ice core. They propose that the northwest GIS is characterized only by a modest reduction of 400 ± 250 m between 128 and 122 kyr BP. In our study, we find at the location of the NEEM ice core an annual mean warming of +9.6°C at 125 kyr BP at a GIS height of 553 m. Antarctic ice cores indicate positive temperature anomalies of up to +3.5°C (Capron et al., 2014), overestimating the simulated TS. However, a reduction in GIS reduces the model-data disagreement.

In order to determine whether a lowered GIS creates a better agreement with the data, we compare the proxy records derived by CAPE Last Interglacial Project Members (2006) to simulation LIG-ctl (Figs. 6c and S4a). We find a better agreement for some records, especially over Greenland where the warming in the simulation LIG-ctl is of a lower magnitude. A high overestimation of reconstructed temperatures by the model is found also by Otto-Bliesner et al. (2006) for a deglaciated Greenland, with summer temperature anomalies being higher than +10°C. Although in our simulations we do not completely remove the ice sheet, we find strong TS anomalies of up to +11°C. The Siberia region experienced similar anomalies in the reconstruction, with records showing +4 to +8°C warming, slightly overestimating our model results. The Arctic Ocean and the North Atlantic Ocean show, in both Otto-Bliesner et al. (2006) and this publication, only modest changes in temperature, mostly underestimating the marine data. The discrepancy is partly removed by considering simulated TS anomalies for maximum summer warmth during the LIG (Fig. 6d).

We go one step further and perform an additional model–data comparison with global coverage (Turney and Jones, 2010). Lunt et al. (2013) performed a model–data comparison for the LIG, using a multi-model approach including our LIG-GHG simulation. None of the model simulations, used in their study, consider a reduction of the GIS elevation or albedo. As in our simulations, Lunt et al. (2013) find that the models fail to capture the magnitude of the temperature anomaly suggested by the proxy data. In their study, the model–data difference is slightly higher than in our study when comparing simulations to terrestrial data, as none of the simulations manage to capture a strong annual

mean warming in the high latitudes. In fact, most of the models suggest a slight cooling over northern Asia at the beginning of the LIG (130 kyr BP) and only a slight warming over Greenland. Over Alaska, the proxy records show a strong warming, which is not captured by any simulation analyzed by Lunt et al. (2013). Our reduced GIS simulation (LIG-1300m-alb) also presents a warming, but of a slightly higher magnitude, reducing the disagreement between model and data. Most of the temperature records in Europe indicate a positive LIG temperature anomaly, whereas the multi-model analysis by Lunt et al. (2013) captures a slight cooling. Another region where reconstructions agree better with our simulated TS is situated over Antarctica, where simulated and reconstructed temperature anomalies indicate a warming of similar magnitude, in contrast to the simulations performed by Lunt et al. (2013), where most of the models indicate a slight cooling. These results imply that a reduced GIS during the LIG may have contributed to an increase in temperature – in our study, the difference between the terrestrial proxy-based temperature anomalies and the anomalies of LIG simulation that implies a PI GIS configuration is higher than when reduced GIS is considered (Fig. 7). The RMSD values support this assumption (Table 2), although differences between the considered cases (i.e. with or without a reduction in GIS) are relatively small. The differences are small because in the calculation of the RMSD, all the proxy records by Turney and Jones (2010) are considered, including a large number of records in the low latitudes where a change in GIS has no influence. Yet, in all simulations the models do not capture the magnitude of the SST anomalies derived from marine records. Such underestimation of proxy data by the models is also found in model–data comparison studies for the Holocene (Masson-Delmotte et al., 2006; Brewer et al., 2007; Sundqvist et al., 2010; Zhang et al., 2010; O'ishi and Abe-Ouchi, 2011; Braconnot et al., 2012; Lohmann et al., 2013; Bakker et al., 2014). Lohmann et al. (2013) show that the simulated SST trends systematically underestimate the marine proxy-based temperature trends, and suggest that such discrepancies can be caused either by too simplistic interpretations of the proxy data (including dating uncertainties and seasonal biases) or by underestimated long-term feedbacks in climate models, a feature which is probably also valid for the LIG. Such long-term feedbacks missing in our model is for example the lithosphere which has not been yet implemented in COSMOS. A coupled ice sheet model and biogeochemistry are already implemented in the COSMOS but are relatively new tools. We did not consider them in our simulations because running the carbon cycle and the ice sheet into equilibrium would take a very long computational time. Additionally, other factors like glacial memory effect is not well represented and cannot be fully reproduced by the models.

Our reduced GIS simulation (LIG-1300m-alb) indicates a strong annual mean warming in the high

latitudes with respect to PI (Fig. 7a). These changes are in accordance with the terrestrial proxy-based temperature anomalies by Turney and Jones (2010), although at northern high latitudes the order of magnitude differs between model and reconstruction, with the model underestimating the reconstructions. The ocean surface in the middle and low latitudes experiences mostly no TS change in our simulation, in contrast to the proxy-based SST anomalies that indicate strong positive or negative temperature changes. Our results partly contradict another early LIG (130 kyr BP) model simulation study performed by Otto-Bliesner et al. (2013). The Community Climate System Model 3 (CCSM3) used in their analysis simulates mostly a cooling in the ocean, with the exception of the North Atlantic Ocean south of Greenland, where the anomalies have the same sign as proxy-based SSTs by Turney and Jones (2010). Terrestrial proxy-based temperatures indicate a better agreement with our simulation, especially over northern Asia, Alaska, and Antarctica. Even when considering mid-LIG (125 kyr BP), in both studies (see Figs. S11 for our study), the terrestrial data can be better reconciled with the simulation in which GIS elevation and albedo are reduced, especially over Antarctica where Otto-Bliesner et al. (2013) find a cooling. Nevertheless, the difference between the magnitude of change in model and reconstruction is still large. One contributing factor to warmer temperatures in the high latitudes in our study may be (as also proposed by Otto-Bliesner et al., 2013) the vegetation feedback, which is considered in our simulations. Over Greenland, the CCSM3 model underestimates the ice record data, while our model simulations LIG-×0.5, LIG-1300m, and LIG-1300m-alb capture an overestimation. Otto-Bliesner et al. (2013) propose that the Greenland ice records may capture temperatures associated with a reduction in GIS elevation. This suggests again that the LIG GIS was lower, but possibly not as low as prescribed in our study. Otto-Bliesner et al. (2013) take into account also possible seasonal biases considered by Lohmann et al. (2013). To this end, they compare the proxy data to simulated JJA temperature anomalies for which they find the best fit, suggesting that the proxies record boreal summer temperatures. In our study, we find the best overall fit for simulated annual mean rather than summer TS (Figs. S11a and S12a) in all three cases: reduced GIS and albedo for beginning of the LIG (LIG-1300m-alb, 130 kyr BP, Figs. 7a and 8b), for mid-LIG (LIG-125k, 125 kyr BP, Figs. S11a, c), and for the control run with prescribed PI GIS (LIG-ctl, 130 kyr BP, Figs. 6c and S4b), with the best agreement between model and data in the first case (Table S2). This could indicate that the proxies may indeed record annual mean temperatures, but in a warmer climate caused by a reduced GIS (Fig. 7a). While the simulated summer TS are closer to the proxies at some locations (e.g. Northern Asia and Europe, Figs. S7a, S8), there are still more records that agree best with the simulated

annual mean TS (Fig. 7a). Otto-Bliesner et al. (2013) include in their study also a mid-LIG simulation performed by Gordon et al. (2000) with the HadCM3 model. Their simulation indicates an even lower agreement between model and data.

4.4 Limitations of model-data comparison

One challenge in an effective LIG model–data comparison is the difficulty to determine an absolute dating of LIG marine paleo-proxy records (e.g. Drysdale et al., 2009), as few techniques exist for this purpose. The dating of most of the records is derived by lining up the climatic signal recorded in sediment cores to the SPECMAP (SPECtral MAping Project, Imbrie et al., 1984; Martinson et al., 1987) reference curve, which is tuned to the June insolation at 65°N. This strategy allows a relative dating of sediment cores through global effects of glacial–interglacial climate changes beyond the time limit of radiocarbon dating (Fairbanks et al., 2005; Chiu et al., 2007; Reimer et al., 2009; Shanahan et al., 2012; Reimer et al., 2013), but it may lead to an artificial synchronization of all records and therefore dampen regional differences in climate records with respect to the LIG chronozone. A relatively new method for synchronizing different types of proxies from different regions is used in Capron et al. (2014). They align proxy records to the AICC2012 ice core chronology allowing for consideration of dating uncertainties. Their study shows that the maximum temperature changes during the LIG is different between the two hemispheres, the records from Southern Ocean and Antarctica showing an early maximum compared to the records from northern high latitudes.

Additionally, some proxy records that are considered as recording annual mean temperatures are seasonally biased, depending on the type of the proxy or on the region (Leduc et al., 2010; Schneider et al., 2010; Lohmann et al., 2013). Furthermore, defining the timing of the maximum warmth during the LIG represents as well a challenge. Different studies (model- as well as proxy-based) suggest that the maximum warmth occurred at different times throughout the LIG with regional dependency (Bakker et al., 2012; Govin et al., 2012; Langebroek and Nisancioglu, 2014). A study that involves transient LIG simulations performed with nine different models is presented by Bakker and Renssen (2014), who find that the calculation of the maximum LIG temperature is largely model-dependent, and also shows geographical- and time-dependency (retrieved values differ between the annual mean and warmest month temperature anomalies). Bakker and Renssen (2014) propose that the time-dependency originates from the dependency of the time evolution of orbital forcing on latitude and seasons, as well as from the thermal inertia of the oceans and from different feedbacks in the climate system, such as the presence of remnant ice sheets from the preceding deglaciation, changes in sea-ice cover, vegetation,

meridional overturning strength, and monsoon dynamics. Our model results indicate that the timing of maximum LIG warmth is indeed regionally dependent (Fig. 9).

5. Conclusions

In this study, we have analyzed data from several LIG sensitivity simulations performed with an atmosphere–ocean general circulation model and assess the influence of the GIS on global climate. We have compared the simulated TS changes to anomalies as recorded by proxy reconstructions by CAPE Last Interglacial Project Members (2006), Turney and Jones (2010), and a compilation of synchronized records by (Capron et al., 2014).

We have shown that the exact method by which GIS configuration is changed has a significant influence on hemispheric temperature anomalies. A reduction in GIS by ~1300 m and changes in albedo (LIG-1300m-alb simulation) enhance the warming caused by changes in the astronomical forcing by up to +5°C. The LIG is much warmer than the PI, especially during summer in the Northern Hemisphere and during winter in the Southern Hemisphere and in the northern high latitudes. The astronomical forcing influence is dominant (relative to changes in GIS) in the global and Northern Hemisphere average of annual mean and local summer TS, and in the Southern Hemisphere winter. Changes in GIS have the strongest influence (relative to insolation changes) globally and in the Northern Hemisphere winter average TS, and in the Southern Hemisphere summer.

Modification of the GIS alone leads to a warming mostly in the northern and southern high latitudes. Cooling occurs locally in Barents Sea or Sea of Okhotsk (depending on the simulation). The warming caused by a reduced GIS has a winter signal, rather than a summer signal at both hemispheres. Winter TS over the Arctic Ocean is warmer by up to +3°C due to GIS changes, with an additional warming of +1 to +2°C caused by winter insolation changes, relative to PI.

The simulated TS underestimate the temperature changes indicated by the proxy reconstructions. However, a reduction in GIS elevation and extent improves the agreement between model and data by Turney and Jones (2006). For terrestrial records, which represent annual mean temperature anomalies at maximum LIG warmth, the best agreement is found for annual mean TS anomalies at maximum LIG warmth derived from the simulation with changes in GIS and albedo (LIG-1300m-alb-tr simulation). This result is in contrast to other model studies that find a best agreement when summer averages are considered At low latitudes the model does not capture the pronounced changes indicated by the marine proxies derived by Turney and Jones (2010). Most of the records derived by CAPE Last Interglacial Project Members (2006) and Capron et al. (2014) agree best with the model simulation that considers a

preindustrial GIS configuration, as changes in GIS have the strongest influence during winter and the respective datasets represent summer temperatures

Throughout the LIG, winter in the northern high latitudes is characterized by high temporal variability, while summer TS indicate a clear cooling trend. By considering transient simulations with different boundary conditions (i.e. GIS elevation, albedo, insolation, GHG concentrations) we offer a bandwidth of potential temperatures at each given time throughout the LIG, between 130 and 115 kyr BP. We reduce the mismatch between model and data by additionally considering uncertainties in absolute dating of the proxy reconstructions, and uncertainties in the timing of maximum LIG warmth (calculated in our study as the simulated maximum LIG warmth between 130 and 120 kyr BP at each given location). The definition of maximum interglacial warmth provides therefore an additional uncertainty and the LIG does not provide a strong constrain for estimating the amplitude of interglacial climate change. Future studies that provide a better multi-proxy interpretation and a better representation of the climate models are needed in order to reduce the model–data mismatch. Our sensitivity simulations represent a starting point for future studies on transient integrations of the LIG climate that include also transient changes in GIS elevation and extent, and for the comparison of such results to high-quality proxy data. More climate model sensitivity studies on the effects of a reduced GIS on global climate are needed in order to understand the response of different models to such changes, as the ability of the models to properly simulate future states of the GIS is critical.

Acknowledgement. This study has been funded by the Deutsche Forschungsgemeinschaft (DFG) under grant agreement no. LO 895/8-1 through priority programme INTERDYNAMIK (SPP 1266) and is part of the project “Evaluation of Eemian and Holocene Climate Variability: Synthesis of marine archives with climate modelling”. We are very grateful to the Anonymous Referee #1 for the constructive comments. We thank very much Emilie Capron for the in-depth and helpful comments and for providing us the proxy-based dataset. We thank Dan Lunt for providing the formatted proxy-based dataset of Turney and Jones (2010). Furthermore, we thank the many contributors for making the temperature proxy-data available.

References

Alley, R. B., Andrews, J. T., Brigham-Grette, J., Clarke, G. K. C., Cuffey, K. M., Fitzpatrick, J. J., Funder, S., Marshall, S. J., Miller, G. H., Mitrovica, J. X., Muhs, D. R., Otto-Bliesner, B. L., Polyak, L., and White, J. W. C.: History of the Greenland Ice Sheet: paleoclimatic insights,

Quaternary Sci. Rev., 29, 1728–1756, doi:16/S0277-3791(99)00062-1, 2010.

Bakker, P. and Renssen, H.: Last Interglacial model–data mismatch of thermal maximum temperatures partially explained, Clim. Past, 9, 1633–1644, doi:10.5194/cpd-10-739-2014, 2014.

Bakker, P., Van Meerbeeck, C. J., and Renssen, H.: Sensitivity of the North Atlantic climate to Greenland Ice Sheet melting during the Last Interglacial, Clim. Past, 8, 995–1009, doi:10.5194/cp-8-995-2012, 2012.

Bakker, P., Stone, E. J., Charbit, S., Gröger, M., Krebs-Kanzow, U., Ritz, S. P., Varma, V., Khon, V., Lunt, D. J., Mikolajewicz, U., Prange, M., Renssen, H., Schneider, B., and Schulz, M.: Last interglacial temperature evolution – a model inter-comparison, Clim. Past, 9, 605–619, doi:10.5194/cp-9-605-2013, 2013.

Bakker, P., Masson-Delmotte, V., Martrat, B., Charbit, S., Renssen, H., Gröger, M., Krebs-Kanzow, U., Lohman, G., Lunt, D. J., Pfeiffer, M., Phipps, S. J., Prange, M., Ritz, S. P., Schulz, M., Stenni, B., Stone, E. J., and Varma, V.: Temperature trends during the Present and Last Interglacial periods – a multi-model–data comparison, Quaternary Sci. Rev., 99, 224–243, doi:10.1016/j.quascirev.2014.06.031, 2014.

Bauch, H. A. and Erlenkeuser, H.: Interpreting glacial–interglacial changes in ice volume and climate from subarctic deep water foraminiferal $\delta^{18}O$, in: Earth's Climate and Orbital Eccentricity: The Marine Isotope Stage 11 Question, edited by: Droxler, A. W., Poore, R. Z., and Burckle, L. H., American Geophysical Union Monograph Series, Washington DC, 87–102, doi:10.1029/137GM07, 2003.

Berger, A. L.: Long-term variations of daily insolation and Quaternary climatic changes, J. Atmos. Sci., 35, 2362–2367, doi:10.1175/1520-0469(1978)035<2362:LTVODI>2.0.CO;2, 1978.

Berger, A. and Loutre, M. F.: Insolation values for the climate of the last 10 million years, Quaternary Sci. Rev., 10, 297–317, doi:10.1016/0277-3791(91)90033-Q, 1991.

Braconnot, P., Otto-Bliesner, B., Harrison, S., Joussaume, S., Peterchmitt, J.-Y., Abe-Ouchi, A., Crucifix, M., Driesschaert, E., Fichefet, Th., Hewitt, C. D., Kageyama, M., Kitoh, A., Loutre, M.-F., Marti, O., Merkel, U., Ramstein, G., Valdes, P., Weber, L., Yu, Y., and Zhao, Y.: Results of PMIP2 coupled simulations of the Mid-Holocene and Last Glacial Maximum – Part 2: feedbacks with emphasis on the location of the ITCZ and mid- and high latitudes heat budget, Clim. Past, 3, 279–296, doi:10.5194/cp-3-279-2007, 2007.

Braconnot, P., Harrison, S., Kageyama, M., Bartlein, P., Masson-Delmotte, V., Abe-Ouchi, A., Otto-Bliesner, B., and Zhao, Y.: Evaluation of climate models using palaeoclimatic data, Nat. Clim. Change, 2, 417–424, doi:10.1038/nclimate1456, 2012.

Brewer, S., Guiot, J., and Torre, F.: Mid-Holocene climate change in Europe: a data-model comparison, Clim. Past, 3, 499–512, doi:10.5194/cp-3-499-2007, 2007.

Brovkin, V., Raddatz, T., Reick, C. H., Claussen, M., and Gayler, V.: Global biogeophysical interactions between forest and climate, Geophys. Res. Lett., 36, L07405, doi:10.1029/2009GL037543, 2009.

CAPE-members – Anderson, P., Bennike, O., Bigelow, N., Brigham-Grette, J., Duvall, M.,

Edwards, M., Fréchette, B., Funder, S., Johnsen, S., Knies, J., Koerner, R., Lozhkin, A., MacDonald, G., Marshall, S., Matthiessen, J., Miller, G., Montoya, M., Muhs, D., Otto-Bliesner, B., Overpeck, J., Reeh, N., Sejrup, H. P., Turner, C., and Velichko, A.: Last Interglacial Arctic warmth confirms polar amplification of climate change, Quaternary Sci. Rev., 25, 1383–1400, doi:10.1016/j.quascirev.2006.01.033, 2006.

Capron, E., Govin, A., Stone, E. J., Masson-Delmotte, V., Mulitza, S., Otto-Bliesner, B. L., Rasmussen, T. L., Sime, L. C., Waelbroeck, C., and Wolff, E. W.: Temporal and spatial structure of multi-millennial temperature changes at high latitudes during the Last Interglacial, Quaternary Sci. Rev., 103, 116–133, doi:10.1016/j.quascirev.2014.08.018, 2014.

Carlson, A. E., Stoner, J. S., Donnelly, J. P., and Hillaire-Marcel, C.: Response of the southern Greenland Ice Sheet during the last two deglaciations, Geology, 36, 359–362, doi:10.1130/G24519A.1, 2008.

Chiu, T.-C., Fairbanks, R. G., Cao, L., and Mortlock, R. A.: Analysis of the atmospheric ^{14}C record spanning the past 50,000 years derived from high-precision $^{230}Th/^{234}U/^{238}U$ and $^{231}Pa/^{235}U$ and ^{14}C dates on fossil corals, Quaternary Sci. Rev., 26, 18–36, doi:10.1016/j.quascirev.2006.06.015, 2007.

Church, J. A., Clark, P. U., Cazenave, A., Gregory, J. M., Jevrejeva, S., Levermann, A., Merrifield, M. A., Milne, G. A., Nerem, R. S., Nunn, P. D., Payne, A. J., Pfeffer, W. T., Stammer, D., and Unnikrishnan, A. S.: Sea level change, in: Climate Change 2013: The Physical Science Basis, Contribution of Working Group I to the Fifth Assessment Report of the Intergovernmental Panel on Climate Change, edited by: Stocker, T. F., Qin, D., Plattner, G.-K., Tignor, M., Allen, S. K., Boschung, J., Nauels, A., Xia, Y., Bex, V., and Midgley, P. M., Cambridge University Press, Cambridge, UK and New York, USA, 1137–1216, 2013.

CLIMAP Project Members: The Last Interglacial ocean, Quaternary Res., 21, 123–224, 1984.

Collins, M., Knutti, R., Arblaster, J., Dufresne, J.-L., Fichefet, T., Friedlingstein, P., Gao, X., Gurowki, W. J., Johns, T., Krinner, G., Shongwe, M., Tebaldi, C., Weaver, A. J., and Wehner, M.: Long-term climate change: projections, commitments and irreversibility, in: Climate Change 2013: The Physical Science Basis, Contribution of Working Group I to the Fifth Assessment Report of the Intergovernmental Panel on Climate Change, edited by: Stocker, T. F., Qin, D., Plattner, G.-K., Tignor, M., Allen, S. K., Boschung, J., Nauels, A., Xia, Y., Bex, V., and Midgley, P. M., Cambridge University Press, Cambridge, UK and New York, USA, 1029–1136, 2013.

Colville, E. J., Carlson, A. E., Beard, B. L., Hatfield, R. G., Stoner, J. S., Reyes, A. V., and Ullman, D. J.: Sr-Nd-Pb isotope evidence for ice-sheet presence on southern Greenland during the last interglacial, Science, 333 (6042), 620–623, doi:10.1126/science.1204673, 2011.

Crowley, T. J. and Kim, K.-Y.: Milankovitch forcing of the Last Interglacial sea level, Science, 265, 1566–1568, 1994.

Cuffey, K. M. and Marshall, S. J.: Substantial contribution to sea-level rise during the last interglacial from the Greenland ice sheet, Nature, 404, 591–594, doi:10.1038/35007053, 2000.

Dahl-Jensen, D., Albert, M. R., Aldahan, A., Azuma, N., Balslev-Clausen, D., Baumgartner, M.,

Berggren, A., Bigler, M., Binder, T., Blunier, T., Bourgeois, J. C., Brook, E. J., Buchardt, S. L., Buizert, C., Capron, E., Chappellaz, J., Chung, J., Clausen, H. B., Cvijanovic, I., Davies, S. M., Ditlevsen, P., Eicher, O., Fischer, H., Fisher, D. A., Fleet, L. G., Gfeller, G., Gkinis, V., Gogineni, S., Goto-Azuma, K., Grinsted, A., Gudlaugsdottir, H., Guillevic, M., Hansen, S. B., Hansson, M., Hirabayashi, M., Hong, S., Hur, S. D., Huybrechts, P., Hvidberg, C. S., Iizuka, Y., Jenk, T., Johnsen, S. J., Jones, T. R., Jouzel, J., Karlsson, N. B., Kawamura, K., Keegan, K., Kettner, E., Kipfstuhl, S., Kjær, H. A., Koutnik, M., Kuramoto, T., Köhler, P., Laepple, T., Landais, A., Langen, P. L., Larsen, L. B., Leuenberger, D., Leuenberger, M., Leuschen, C., Li, J., Lipenkov, V., Martinerie, P., Maselli, O. J., Masson-Delmotte, V., McConnell, J. R., Miller, H., Mini, O., Miyamoto, A., Montagnat-Rentier, M., Mulvaney, R., Muscheler, R., Orsi, A. J., Paden, J., Panton, C., Pattyn, F., Petit, J., Pol, K., Popp, T., Possnert, G., Prié, F., Prokopiou, M., Quiquet, A., Rasmussen, S. O., Raynaud, D., Ren, J., Reutenauer, C., Ritz, C., Röckmann, T., Rosen, J. L., Rubino, M., Rybak, O., Samyn, D., Sapart, C. J., Schilt, A., Schmidt, A. M. Z., Schwander, J., Schüpbach, S., Seierstad, I., Severinghaus, J. P., Sheldon, S., Simonsen, S. B., Sjolte, J., Solgaard, A. M., Sowers, T., Sperlich, P., Steen-Larsen, H. C., Steffen, K., Steffensen, J. P., Steinhage, D., Stocker, T. F., Stowasser, C., Sturevik, A. S., Sturges, W. T., Sveinbjörnsdottir, A., Svensson, A., Tison, J., Uetake, J., Vallelonga, P., van de Wal, R. S. W., van der Wel, G., Vaughn, B. H., Vinther, B., Waddington, E., Wegner, A., Weikusat, I., White, J. W. C., Wilhelms, F., Winstrup, M., Witrant, E., Wolff, E. W., Xiao, C., and Zheng, J.: Eemian interglacial reconstructed from a Greenland folded ice core, Nature, 493, 489–494, doi:10.1038/nature11789, 2013.

Dowsett, H. J., Foley, K. M., Stoll, D. K., Chandler, M. A., Sohl, L. E., Bentsen, M., Otto-Bliesner, B. L., Bragg, F. J., Chan, W.-L., Contoux, C., Dolan, A. M., Haywood, A. M., Jonas, J. A., Jost, A., Kamae, Y., Lohmann, G., Lunt, D. J., Nisancioglu, K. H., Abe-Ouchi, A., Ramstein, G., Riesselman, C. R., Robinson, M. M., Rosenbloom, N. A., Salzmann, U., Stepanek, C., Strother, S. L., Ueda, H., Yan, Q., and Zhang, Z.: Sea surface temperature of the mid-Piacenzian ocean: a data-model comparison, Scientific Reports, 3, 2013, doi:10.1038/srep02013, 2013.

Drysdale, R. N., Hellstrom, J. C., Zanchetta, G., Fallick, A. E., Sánchez-Goñi, M. F., Couchoud, I., McDonald, J., Maas, R., Lohmann, G., and Isola, I.: Evidence for obliquity forcing of glacial Termination II, Science, 325, 1527–1531, doi:10.1126/science.1170371, 2009.

Dutton, A. and Lambeck, K.: Ice volume and sea level during the last interglacial, Science, 337, 216–219, doi:10.1126/science.1205749, 2012.

Eugster, W., Rouse, W., Pielke Sr., R. A., McFadden, J. P., Baldocchi, D., Kittel, D., Chapin III, T. G. F., Liston, F. S., Vidale, G. E., Vaganov, P. L., and Chambers, E. S.: Land-atmosphere energy exchange in Arctic tundra and boreal forest: available data and feedbacks to climate, Global Change Biol., 6, 84–115, doi:10.1046/j.1365-2486.2000.06015.x, 2000.

Fairbanks, R. G., Mortlock, R. A., Chiu, T.-C., Cao, L., Kaplan, A., Guilderson, T. P., Fairbanks, T. W., Bloom, A. L., Grootes, P. M., and Nadeau, M.-J.: Radiocarbon calibration curve spanning 0 to 50,000 years BP based on paired $^{230}Th/^{234}U/^{238}U$ and ^{14}C dates on pristine corals, Quaternary Sci. Rev., 24, 1781–1796, doi:10.1016/j.quascirev.2005.04.007, 2005.

Felis, T., Lohmann, G., Kuhnert, H., Lorenz, S. J., Scholz, D., Pätzold, J., Al Rousan, S. A., and Al-Moghrabi, S. M.: Increased seasonality in Middle East temperatures during the last interglacial period, Nature, 429, 164–168, doi:10.1038/nature02546, 2004.

Felis, T., Giry, C., Scholz, D., Lohmann, G., Pfeiffer, M., Pätzold, J., Kölling, M., and Scheffers, S. R.: Tropical Atlantic temperature seasonality at the end of the last interglacial, Nature Comm., 6, 6159, doi:10.1038/ncomms7159, 2015.

Fitzjarrald, D. R. and Moore, K. E.: Turbulent transport over tundra, J. Geophys. Res.-Atmos., 97, 16717–16729, doi:10.1029/91JD01030, 1992.

Flato, G., Marotzke, J., Abiodun, B., Braconnot, P., Chou, S. C., Collins, W., Cox, P., Driouech, F., Emori, S., Eyring, V., Forest, C., Gleckler, P., Guilyardi, E., Jakob, C., Kattsov, V., Reason, C., and Rummukainen, M.: Evaluation of climate models, in: Climate Change 2013: The Physical Science Basis, Contribution of Working Group I to the Fifth Assessment Report of the Intergovernmental Panel on Climate Change, edited by: Stocker, T. F., Qin, D., Plattner, G.-K., Tignor, M., Allen, S. K., Boschung, J., Nauels, A., Xia, Y., Bex, V., and Midgley, P. M., Cambridge University Press, Cambridge, UK and New York, USA, 741–866, 2013.

Gauss, C. F. and Stewart, G. W.: Theory of the Combination of Observations Least Subject to Error: Part One, Part Two, Supplement, vol. 11, Classics in Applied Mathematics, Society for Industrial and Applied Mathematics, doi:10.1137/1.9781611971248, 1995.

Gierz, P., Lohmann, G., and Wei, W.: Response of Atlantic overturning to future warming in a coupled atmosphere ocean-ice sheet model, P. Natl. Acad. Sci. USA, submitted, 2015.

Gong, X., Knorr, G., Lohmann, G., and Zhang, X.: Dependence of abrupt Atlantic meridional ocean circulation changes on climate background states, Geophys. Res. Lett., 40, 3698–3704, doi:10.1002/grl.50701, 2013.

Gong, X., Zhang, X., Lohmann, G., Wei, W., Zhang, Xu, and Pfeiffer, M.: Higher Laurentide and Greenland ice sheets strengthen the North Atlantic ocean circulation, Clim. Dynam., 1–12, doi:10.1007/s00382-015-2502-8, 2015.

Gordon, C., Cooper, C., Senior, C. A., Banks, H., Gregory, J. M., Johns, T. C., Mitchell, J. F. B., and Wood, R. A.: The simulation of SST, sea ice extents and ocean heat transports in a version of the Hadley Centre coupled model without flux adjustments, Clim. Dynam., 16, 147–168, doi:10.1007/s003820050010, 2000.

Govin, A., Braconnot, P., Capron, E., Cortijo, E., Duplessy, J.-C., Jansen, E., Labeyrie, L., Landais, A., Marti, O., Michel, E., Mosquet, E., Risebrobakken, B., Swingedouw, D., and Waelbroeck, C.: Persistent influence of ice sheet melting on high northern latitude climate during the early Last Interglacial, Clim. Past, 8, 483–507, doi:10.5194/cp-8-483-2012, 2012.

Harrison, S. P., Kutzbach, J. E., Prentice, C. E., Behling, P. J., and Sykes, M. T.: The response of Northern Hemisphere extratropical climate and vegetation to orbitally induced changes in insolation during the last interglaciation, Quaternary Res., 43, 174–184, doi:10.1006/qres.1995.1018, 1995.

Herold, M. and Lohmann, G.: Eemian tropical and subtropical African moisture transport: an isotope modelling study, Clim. Dynam., 33, 1075–1088, doi:10.1007/s00382-008-0515-2, 2009.

Hibler, W.: Dynamic thermodynamic sea ice model, J. Phys. Oceanogr., 9, 815–846, 1979.

Imbrie, J., Hays, J. D., Martinson, D. G., McIntyre, A., Mix, A. C., Morley, J. J., Paces, N. G., Prell,

W. L., and Shackleton, N. J.: The orbital theory of Pleistocene climate: support from a revised chronology of the marine d^{18}O record, in: Milankovitch and Climate, Part I, edited by: Berger, A. L., Imbrie, J., Hays, J. D., Kukla, G., and Saltzman, B., D. Reidel, Dordrecht, the Netherlands, 269–305, 1984.

Jansen, E., Overpeck, J., Briffa, K. R., Duplessy, J.-C., Joos, F., Masson-Delmotte, V., Olago, D., Otto-Bliesner, B., Peltier, W. R., Rahmstorf, S., Ramesh, R., Raynaud, D., Rind, D., Solomina, O., Villalba, R., and Zhang, D.: Palaeoclimate, in: Climate Change 2007: The Physical Science Basis, Contribution of Working Group I to the Fourth Assessment Report of the Intergovernmental Panel on Climate Change, edited by: Solomon, S., Qin, D., Manning, M., Chen, Z., Marquis, M., Averyt, K. B., Tignor, M., and Miller, H. L., Cambridge University Press, Cambridge, UK and New York, USA, 433–497, 2007.

Jennings, R., Singarayer, J., Stone, E. J., Krebs-Kanzow, U., Khon, V., Nisancioglu, K. H., Pfeiffer, M., Zhang, X., Parker, A. G., Parton, A., Groucutt, H. S., White, T. S., Drake, N. A., and Petraglia, M. D.: The greening of Arabia: multiple opportunities for human occupation of the Arabian Peninsula during the Late Pleistocene inferred from an ensemble of climate model simulations, Quatern. Int., 1–19, doi:10.1016/j.quaint.2015.01.006, 2015.

Johnsen, S. J. and Vinther, B. M.: Greenland stable isotopes, in: Encyclopedia of Quaternary Science, Elsevier, 1250–1258, doi:10.1016/B0-444-52747-8/00345-8, 2007.

Johnsen, S. J., Dahl-Jensen, D., Gundestrup, N., Steffensen, J.-P., Clausen, H. B., Miller, H., Masson-Delmotte, V., Sveinbjornsdottir, A. E., and White, J.: Oxygen isotope and palaeotemperature records from six Greenland ice-core stations: Camp Century, Dye-3, GRIP, GISP2, Renland and NorthGRIP, J. Quaternary Sci., 16, 299–307, doi:10.1002/jqs.622, 2001.

Jungclaus, J. H., Keenlyside, N., Botzet, M., Haak, H., Luo, J. J., Latif, M., Marotzke, J., Mikolajewicz, U., and Roeckner, E.: Ocean circulation and tropical variability in the coupled model ECHAM5/MPI-OM, J. Climate, 19, 3952–3972, doi:10.1175/JCLI3827.1, 2006.

Kaspar, F. and Cubasch, U.: Simulations of the Eemian interglacial and the subsequent glacial inception with a coupled ocean atmosphere general circulation model, in: The Climate of Past Interglacials, edited by: Sirocko, F., Litt, T., Claussen, M., and Sánchez-Goñi, M. F., Elsevier, Developments in Quaternary Sciences, 7, Chap. 33, 499–515, doi:10.1016/S1571-0866(07)80058-3, 2007.

Kaspar, F., Kühl, N., Cubasch, U., and Litt, T.: A model–data comparison of European temperatures in the Eemian interglacial, Geophys. Res. Lett., 32, L11703, doi:10.1029/2005GL022456 , 2005.

Kirtman, B., Power, S. B., Adedoyin, J. A., Boer, G. J., Bojariu, R., Camilloni, I., Doblas-Reyes, F. J., Fiore, A. M., Kimoto, M., Meehl, G. A., Prather, M., Sarr, A., Schär, C., Sutton, R., van Oldenborgh, G. J., Vecchi, G., and Wang, H. J.: Near-term climate change: projections and predictability, in: Climate Change 2013: The Physical Science Basis. Contribution of Working Group I to the Fifth Assessment Report of the Intergovernmental Panel on Climate Change, edited by: Stocker, T. F., Qin, D., Plattner, G.-K., Tignor, M., Allen, S. K., Boschung, J., Nauels, A., Xia, Y., Bex, V., and Midgley, P. M., Cambridge University Press, Cambridge, UK and New York, USA, 953–1028, 2013.

Knorr, G. and Lohmann, G.: A warming climate during the Antarctic ice sheet growth at the Middle

Miocene transition, Nat. Geosci., 7, 376–381, doi:10.1038/NGEO2119, 2014.

Knorr, G., Butzin, M., Micheels, A., and Lohmann, G.: A warm Miocene climate at low atmospheric CO_2 levels, Geophys. Res. Lett., 38, L20701, doi:10.1029/2011GL048873, 2011.

Koerner, R. M.: Ice-core evidence for extensive melting of the Greenland Ice Sheet in the last interglacial, Science, 244, 964–968, 1989.

Koerner, R. M. and Fisher, D. A.: Ice-core evidence for widespread Arctic glacier retreat in the last interglacial and the early Holocene, Ann. Glaciol., 35, 19–24, doi:10.3189/172756402781817338, 2002.

Kopp, R. E., Simons, F. J., Mitrovica, J. X., Maloof, A., and Oppenheimer, M.: Probabilistic assessment of sea level during the last interglacial stage, Nature, 462, 863–867, doi:10.1038/nature08686, 2009.

Kopp, R. E., Simons, F. J., Mitrovica, J. X., Maloof, A., and Oppenheimer, M.: Probabilistic assessment of sea level variations within the last interglacial stage, Geophys. J. Int., 193, 711–716, doi:10.1093/gji/ggt029, 2013.

Kukla, G. J., Bender, M. L., de Beaulieu, J. L., Bond, G., Broecker, W. S., Cleveringa, P., Gavin, J. E., Herbert, T. D., Imbrie, J., Jouzel, J., Keigwin, L. D., Knudsen, K.-L., McManus, J. F., Merkt, J., Muhs, D. R., Müller, H., Poore, R. Z., Porter, S. C., Seret, G., Shackleton, N. J., Turner, C., Tzedakis, P. C., and Winograd, I. J.: Last interglacial climates, Quaternary Res., 58, 2–13, doi:10.1006/qres.2001.2316, 2002.

Kutzbach, J. E., Gallimore, R. G., and Guetter, P. J.: Sensitivity experiments on the effect o orbitally-caused insolation changes on the interglacial climate of high northern latitudes, Quatern. Int., 10–12, 223–229, doi:10.1016/1040-6182(91)90054-R, 1991.

Langebroek, P. M. and Nisancioglu, K. H.: Simulating last interglacial climate with NorESM: role of insolation and greenhouse gases in the timing of peak warmth, Clim. Past, 10, 1305–1318, doi:10.5194/cp-10-1305-2014, 2014.

Laskar, J., Robutel, P., Joutel, F., Gastineau, M., Correia, A. C. M., and Levrard, B.: A long-term numerical solution for the insolation quantities of the Earth, Astron. Astrophys., 428, 261–285, doi:10.1051/0004-6361:20041335, 2004.

Leduc, G., Schneider, R. R., Kim, J. H., and Lohmann, G.: Holocene and Eemian sea surface temperature trends as revealed by alkenone and Mg/Ca paleothermometry, Quaternary Sci. Rev., 29, 989–1004, doi:10.1016/j.quascirev.2010.01.004, 2010.

Lhomme, N., Clarke, G. K. C., and Ritz, C.: (2005): Global budget of water isotopes inferred from polar ice sheets, Geophys. Res. Lett., 32, L20502, doi:10.1029/ 2005GL023774, 2005.

Lohmann, G. and Lorenz, S. J.: Orbital forcing on atmospheric dynamics during the last interglacial and glacial inception, in: The Climate of Past Interglacials, edited by: Sirocko, F., Claussen, M., Sánchez-Goñi, M. F., and Litt, T., Elsevier, Developments in Quaternary Science, 7, 527–546, 2007.

Lohmann, G., Pfeiffer, M., Laepple, T., Leduc, G., and Kim, J.-H.: A model–data comparison of the Holocene global sea surface temperature evolution, Clim. Past, 9, 1807–1839, doi:10.5194/cp-9-1807-2013, 2013.

Lorenz, S. J. and Lohmann, G.: Acceleration technique for Milankovitch type forcing in a coupled atmosphere–ocean circulation model: method and application for the Holocene, Clim. Dynam., 23, 727–743, doi:10.1007/s00382-004-0469-y, 2004.

Loulergue, L., Schilt, A., Spahni, R., Masson-Delmotte, V., Blunier, T., Lemieux, B., Barnola, J.-M., Raynaud, D., Stocker, T. F., and Chappellaz, J.: Orbital and millennial-scale features of atmospheric CH_4 over the past 800,000 years, Nature, 453, 383–386, doi:10.1038/nature06950, 2008.

Loutre, M. F., Fichefet, T., Goosse, H., Huybrechts, P., Goelzer, H., and Capron, E.: Factors controlling the last interglacial climate as simulated by LOVECLIM1.3, Climate of the Past, 10, 1541–1565, doi:10.5194/cp-10-1541-2014, 2014.

Lüthi, D., Le Floch, M., Bereiter, B., Blunier, T., Barola, J. M., Siegenthaler, U., Raynaud, D., Jouzel, J., Fischer, H., Kawamur, K., and Stocker, T. F.: High-resolution carbon dioxide concentration record 650,00–800,000 years before present, Nature, 453, 379–382, doi:10.1038/nature06949, 2008.

Lunt, D. J., Abe-Ouchi, A., Bakker, P., Berger, A., Braconnot, P., Charbit, S., Fischer, N., Herold, N., Jungclaus, J. H., Khon, V. C., Krebs-Kanzow, U., Langebroek, P. M., Lohmann, G., Nisancioglu, K. H., Otto-Bliesner, B. L., Park, W., Pfeiffer, M., Phipps, S. J., Prange, M., Rachmayani, R., Renssen, H., Rosenbloom, N., Schneider, B., Stone, E. J., Takahashi, K., Wei, W., Yin, Q., and Zhang, Z. S.: A multi-model assessment of last interglacial temperatures, Clim. Past, 9, 699–717, doi:10.5194/cp-9-699-2013, 2013.

Marsland, S. J., Haak, H., Jungclaus, J. H., Latif, M., and Röske, F.: The Max-Planck-Institute global ocean/sea ice model with orthogonal curvilinear coordinates, Ocean Model., 5, 91–127, doi:10.1016/S1463-5003(02)00015-X, 2003.

Martinson, D. G., Pisias, N. G., Hays, J. D., Imbrie, J., Moore, T. C., and Shackleton, N.: Age dating and the orbital theory of the ice ages: development of a high-resolution 0 to 300,000 year chronostratigraphy, Quaternary Res., 27, 1–29, doi:10.1016/0033-5894(87)90046-9, 1987.

Masson-Delmotte, V., Kageyama, M., Braconnot, P., Charbit, S., Krinner, G., Ritz, C., Guilyardi, E., Jouzel, J., Abe-Ouchi, A., Crucifix, M., Gladstone, R. M., Hewitt, C. D., Kitoh, A., LeGrande, A. N., Marti, O., Merkel, U., Motoi, T., Ohgaito, R., Otto-Bliesner, B., Peltier, W. R., Ross, I., Valdes, P. J., Vettoretti, G., Weber, S. L., Wolk, F., and Yu, Y.: Past and future polar amplification of climate change: climate model intercomparisons and ice-core constraints, Clim. Dynam., 26, 513–529, doi:10.1007/s00382-005-0081-9, 2006.

Masson-Delmotte, V., Schulz, M., Abe-Ouchi, A., Beer, J., Ganopolski, A., González Rouco, J. F., Jansen, E., Lambeck, K., Luterbacher, J., Naish, T., Osborn, T., Otto-Bliesner, B., Quinn, T., Ramesh, R., Rojas, M., Shao, X., and Timmermann, A.: Information from Paleoclimate archives, in: Climate Change 2013: The Physical Science Basis, Contribution of Working Group I to the Fifth Assessment Report of the Intergovernmental Panel on Climate Change, edited by: Stocker, T. F., Qin, D., Plattner, G.-K., Tignor, M., Allen, S. K., Boschung, J., Nauels, A., Xia, Y., Bex, V., and Midgley, P. M., Cambridge University Press, Cambridge, UK and New York, USA, 383–464, 2013.

McKay, N. P., Overpeck, J. T., and Otto-Bliesner, B. L.: The role of ocean thermal expansion in

Last Interglacial sea level rise, Geophys. Res. Lett., 38, L14605, doi:10.1029/2011GL048280, 2011.

Mearns, L. O., Hulme, M., Carter, T. R., Leemans, R., Lal, M., and Whetton, P.: Climate scenario development, in: Climate Change 2001: The Scientific Basis, Contribution of Working Group I to the Third Assessment Report of the Intergovernmental Panel on Climate Change, edited by: Houghton, J. T., Ding, Y., Griggs, D. J., Noguer, M., van der Linden, P. J., Dai, X., Maskell, K., and Johnson, C. A., Cambridge University Press, Cambridge, UK and New York, USA, 739–768, 2001.

Merz, N., Born, A., Raible, C. C., Fischer, H., and Stocker, T. F.: Dependence of Eemian Greenland temperature reconstructions on the ice sheet topography, Clim. Past, 10, 1221–1238, doi:10.5194/cp-10-1221-2014, 2014.

Montoya, M., von Storch, H., and Crowley, T. J.: Climate simulation for 125 kyr BP with a coupled ocean–atmosphere general circulation model, J. Climate, 13, 1057–1071, doi:10.1175/1520-0442(2000)013<1057:CSFKBW>2.0.CO;2, 2000.

Mudelsee, M.: Climate Time Series Analysis, Classical Statistical and Bootstrap Methods, Atmospheric and Oceanographic Sciences Library, vol. 42, Springer, Dordrecht, 2010.

New, M., Hulme, M., and Jones, P.: Representing twentieth-century space–time climate variability, Part I: Development of a 1961–90 mean monthly terrestrial climatology, J. Climate, 12, 829–856, doi:10.1175/1520-0442(1999)012<0829:RTCSTC>2.0.CO;2, 1999.

North Greenland Ice Core Project members: high-resolution record of Northern Hemisphere climate extending into the last interglacial period, Nature, 431, 147–151, doi:10.1038/nature02805, 2004.

O'ishi, R. and Abe-Ouchi, A.: Polar amplification in the mid-Holocene derived from dynamical vegetation change with a GCM, Geophys. Res. Lett., 38, L14702, doi:10.1029/2011GL048001, 2011.

Otto-Bliesner, B. L., Marshall, S. J., Overpeck, J. T., Miller, G. H., Hu, A., and CAPE Last Interglacial Project members: simulating Arctic Climate Warmth and Icefield Retreat in the Last Interglaciation, Science, 311, 1751–1753, doi:10.1126/science.1120808, 2006.

Otto-Bliesner, B. L., Rosenbloom, N., Stone, E. J., McKay, N. P., Lunt, D. J., Brady, E. C., and Overpeck, J. T.: How warm was the last interglacial? New model – data comparisons, Philos. T. R. Soc. A, 371, 1–20, doi:10.1098/rsta.2013.0097, 2013.

Overpeck, J. T., Otto-Bliesner, B. L., Miller, G. H., Muhs, D. R., Alley, R. B., and Kiehl, J. T.: Paleoclimatic evidence for future ice-sheet instability and rapid sea-level rise, Science, 311, 1747–1750, doi:10.1126/science.1115159, 2006.

Pfeiffer, M. and Lohmann, G.: The Last Interglacial as simulated by an Atmosphere-Ocean General Circulation Model: sensitivity studies on the influence of the Greenland Ice Sheet, in: Earth System Science: bridging the Gaps between Disciplines Perspectives from a Multi-disciplinary Helmholtz Research School, edited by: Lohmann, G., Grosfeld, K., Wolf-Gladrow, D., Unnithan, V., Notholt, J., and Wegner, A., Series: SpringerBriefs in Earth System Sciences, 57–64, Springer, Heidelberg, doi:10.1007/978-3-642-32235-8, 2013.

Quiquet, A., Ritz, C., Punge, H. J., and Salas y Mélia, D.: Greenland ice sheet contribution to sea level rise during the last interglacial period: a modelling study driven and constrained by ice core data, Clim. Past, 9, 353–366, doi:10.5194/cp-9-353-2013, 2013.

Raddatz, T. J., Reick, C. H., Knorr, W., Kattge, J., Roeckner, E., Schnur, R., Schnitzler, K. G., Wetzel, P., and Jungclaus, J.: Will the tropical land biosphere dominate the climate-carbon cycle feedback during the twenty-first century?, Clim. Dynam., 29, 565–574, doi:10.1007/s00382-007-0247-8, 2007.

Reimer, P. J., Baillie, M. G. L., Bard, E., Bayliss, A., Beck, J. W., Blackwell, P. G., Bronk Ramsey, C., Buck, C. E., Burr, G. S., Edwards, R. L., Friedrich, M., Grootes, P. M., Guilderson, T. P., Hajdas, I., Heaton, T. J., Hogg, A. G., Hughen, K. A., Kaiser, K. F., Kromer, B., McCormac, F. G., Manning, S. W., Reimer, R. W., Richards, D. A., Southon, J. R., Talamo, S., Turney, C. S. M., van der Plicht, J., and Weyhenmeyer, C. E.: IntCal09 and Marine09 radiocarbon age calibration curves, 0–50,000 years cal BP, Radiocarbon, 51, 1111–1150, 2009.

Reimer, P. J., Bard, E., Bayliss, A., Beck, J. W., Blackwell, P. G., Bronk Ramsey, C., Buck, C. E., Cheng, H., Edwards, R. L., Friedrich, M., Grootes, P. M., Guilderson, T. P., Haflidason, H., Hajdas, I., Hatté, C., Heaton, T. J., Hoffmann, D. L., Hogg, A. G., Hughen, K. A., Kaiser, K. F., Kromer, B., Manning, S. W., Niu, M., Reimer, R. W., Richards, D. A., Scott, E. M., Southon, J. R., Staff, R. A., Turney, C. S. M., and van der Plicht, J.: IntCal13 and Marine13 radiocarbon age calibration curves 0–50,000 years cal BP, Radiocarbon, 55, 1869–1887, doi:10.2458/azu_js_rc.55.16947, 2013.

Renssen, H., Goosse, H., Fichefet, T., Masson-Delmotte, V., and Koç, N: The Holocene climate evolution in the high-latitude Southern Hemisphere simulated by a coupled atmosphere-sea ice-ocean-vegetation model, Holocene, 15, 951–964, doi:10.1191/0959683605hl869ra, 2005.

Robinson, A., Calov, R., and Ganopolski, A.: Greenland ice sheet model parameters constrained using simulations of the Eemian Interglacial, Clim. Past, 7, 381–396, doi:10.5194/cp-7-381-2011, 2011.

Roeckner, E., Bäuml, G., Bonaventura, L., Brokopf, R., Esch, M., Giorgetta, M., Hagemann, S., Kirchner, I., Kornblueh, L., Manzini, E., Rhodin, A., Schlese, U., Schulzweida, U., and Tompkins, A.: The atmospheric general circulation model ECHAM5, Part I: Model description, Tech. Rep. 349, Max Planck Institute for Meteorology, Hamburg, Germany, 2003.

Schneider, B., Leduc, G., and Park, W.: Disentangling seasonal signals in Holocene climate trends by satellite-model-proxy integration, Paleoceanography, 25, PA4217, doi:10.1029/2009PA001893, 2010.

Semtner, A. J.: A model for the thermodynamic growth of sea ice in numerical investigations of climate, J. Phys. Oceanogr., 6, 379–389, 1976.

Shanahan, T. M., Beck, J. W., Overpeck, J. T., McKay, N. P., Pigati, J. S., Peck, J. A., Scholz, C. A., Heil Jr., C. W., and King, J.: Late Quaternary sedimentological and climate changes at Lake Bosumtwi Ghana: new constraints from laminae analysis and radiocarbon age modeling, Palaeogeogr. Palaeocl., 361–362, 49–60, doi:10.1016/j.palaeo.2012.08.001, 2012.

Smith, T. M. and Reynolds, R. W.: A high-resolution global sea surface temperature climatology for

the 1961–90 base period, J. Climate, 11, 3320–3323, doi:10.1175/1520-0442(1998)011<3320:AHRGSS>2.0.CO;2, 1998.

Spahni, R., Chappellaz, J., Stocker, T. F., Loulergue, L., Hausammann, G., Kawamura, K., Fluckiger, J., Schwander, J., Raynaud, D., Masson-Delmotte, V., and Jouzel, J.: Atmospheric methane and nitrous oxide of the late Pleistocene from Antarctic ice cores, Science, 310, 1317–1321, doi:10.1126/science.1120132, 2005.

Stepanek, C. and Lohmann, G.: Modelling mid-Pliocene climate with COSMOS, Geosci. Model Dev., 5, 1221–1243, doi:10.5194/gmd-5-1221-2012, 2012.

Stirling, C. H., Esat, T. M., Lambeck, K., and McCulloch, M. T.: Timing and duration of the last interglacial: evidence for a restricted interval of widespread coral reef growth, Earth Planet. Sc. Lett., 160, 745–762, doi:10.1016/S0012-821X(98)00125-3, 1998.

Stone, E. J., Lunt, D. J., Annan, J. D., and Hargreaves, J. C.: Quantification of the Greenland ice sheet contribution to Last Interglacial sea level rise, Clim. Past, 9, 621–639, doi:10.5194/cp-9-621-2013, 2013.

Sundqvist, H. S., Zhang, Q., Moberg, A., Holmgren, K., Körnich, H., Nilsson, J., and Brattström, G.: Climate change between the mid and late Holocene in northern high latitudes – Part 1: Survey of temperature and precipitation proxy data, Clim. Past, 6, 591–608, doi:10.5194/cp-6-591-2010, 2010.

Tarasov, L. and W. R. Peltier: Greenland glacial history, borehole constraints, and Eemian extent, J. Geophys. Res., 108(B3), 2143, doi:10.1029/2001JB001731, 2003.

Turney, C. S. M. and Jones, R. T.: Does the Agulhas current amplify global temperatures during super-interglacials?, J. Quaternary Sci., 25, 839–843, doi:10.1002/Jqs.1423, 2010.

Valcke, S.: The OASIS3 coupler: a European climate modelling community software, Geosci. Model Dev., 6, 373–388, doi:10.5194/gmd-6-373-2013, 2013.

Valcke, S., Caubel, A., Declat, D., and Terray, L.: OASIS Ocean Atmosphere Sea Ice Soil users guide, Tech. Rep. TR/CMGC/03-69, CERFACS, Toulouse, France, 2003.

van de Berg, W. J., van den Broeke, M., Ettema, J., van Meijgaard, E., and Kaspar, F.: Significant contribution of insolation to Eemian melting of the Greenland ice sheet, Nat. Geosci., 4, 679–683, doi:10.1038/ngeo1245, 2011.

Veeh, H. H.: Th^{230}/U^{238} and U^{234}/U^{238} ages of Pleistocene high sea level stand, J. Geophys. Res., 71, 3379–3386, 1966.

von Storch, H. and Zwiers, F. W.: Statistical Analysis in Climate Research, Cambridge University Press, New York, 1999.

Wei, W. and Lohmann, G.: Simulated Atlantic Multidecadal Oscillation during the Holocene, J. Climate, 25, 6989–7002, doi:10.1175/JCLI-D-11-00667.1, 2012.

Wei, W., Lohmann, G., and Dima, M.: Distinct modes of internal variability in the global meridional overturning circulation associated with the SH westerly winds, J. Phys. Oceanogr., 42, 785–801, doi:10.1175/JPO-D-11-038.1, 2012.

Willerslev, E., Cappellini, E., Boomsma, W., Nielsen, R., Hebsgaard, M. B., Brand, T. B., Hofreiter,

M., Bunce, M., Poinar, H. N., Dahl-Jensen, D., Johnsen, S., Steffensen, J. P., Bennike, O., Schwenninger, J.-L., Nathan, R., Armitage, S., de Hoog, C.-J., Alfimov, V., Christl, M., Beer, J., Muscheler, R., Barker, J., Sharp, M., Penkman, K. E. H., Haile, J., Taberlet, P., Gilbert, M. T. P., Casoli, A., Campani, E., and Collins, M. J.: Ancient bio-molecules from deep ice cores reveal a forested southern Greenland, Science, 317, 111–114, doi:10.1126/science.1141758, 2007.

Yin, Q. Z. and Berger, A.: Insolation and CO_2 contribution to the interglacial climate before and after the Mid-Brunhes Event, Nat. Geosci., 3, 243–246, doi:10.1038/ngeo771, 2010.

Zhang, Q., Sundqvist, H. S., Moberg, A., Körnich, H., Nilsson, J., and Holmgren, K.: Climate change between the mid and late Holocene in northern high latitudes – Part 2: Model-data comparisons, Clim. Past, 6, 609–626, doi:10.5194/cp-6-609-2010, 2010.

Zhang, X., Lohmann, G., Knorr, G., and Xu, X.: Different ocean states and transient characteristics in Last Glacial Maximum simulations and implications for deglaciation, Clim. Past, 9, 2319–2333, doi:10.5194/cp-9-2319-2013, 2013.

Zhang, X., Lohmann, G., Knorr, G., and Purcell, C.: Control of rapid glacial climate shifts by variations in intermediate ice-sheet volume, Nature, 512, 290–294, doi:10.1038/nature13592, 2014.

Table and Figure captions

Table 1. Overview of model configuration and climate forcings for the COSMOS simulations presented in this study. PI = preindustrial, Veg. = vegetation; dyn. = dynamic; e = eccentricity; ε = obliquity; ω = length of perihelion. The Greenland Ice Sheet (GIS) configuration is, in dependence of the simulation, as follows: PI – preindustrial GIS elevation and land ice mask; ×0.5 – preindustrial GIS elevation multiplied by 0.5 (at every grid point over Greenland) and preindustrial land ice mask; −1300 m – preindustrial GIS elevation minus 1300 m (at every grid point over Greenland; where preindustrial elevation is below 1300 m, the land is set to 0 m) and preindustrial land ice mask; −1300 m+alb – preindustrial GIS elevation minus 1300 m (at every grid point over Greenland; where preindustrial elevation is below 1300 m, the land is set to 0 m and albedo adjusted accordingly) and adjusted land ice mask. The different GIS configurations are displayed in Fig. 1. * Simulations that are presented in the supplementary material.

Table 2. Atlantic Meridional Overturning Circulation (AMOC) and absolute values of surface temperature (TS) for global, Northern Hemisphere (NH), and Southern Hemisphere (SH) coverage, calculated for annual mean, local summer mean (warmest month), and local winter mean (coldest month).

Figure 1. Greenland Ice Sheet (GIS) elevation (in m) and land ice cover prescribed in our COSMOS model simulations: **(a)** preindustrial GIS and land ice mask, **(b)** ×0.5 GIS and preindustrial land ice mask, **(c)** −1300 m GIS and preindustrial land ice mask, **(d)** −1300 m and adjusted land ice mask. In **(a),** the preindustrial elevation and land ice mask are unchanged. In **(b),** the preindustrial elevation over the GIS area is multiplied by 0.5; the land ice mask is unchanged. In **(c)**, for each grid point over the GIS, 1300 m are subtracted from preindustrial elevation; the land ice mask is unchanged. In **(d),** for each grid point over the GIS, 1300 m are subtracted from preindustrial elevation; at grid locations where the elevation is lower than 1300 m, land ice is removed and albedo is adjusted accordingly.

Figure 2. Effect of **(a–c)** Greenland Ice Sheet elevation and **(c, d)** albedo in the 130 kyr BP simulations. Annual mean surface temperature (TS) anomalies (in °C) for simulations: **(a)** LIG-×0.5 minus LIG-ctl, **(b)** LIG-1300m minus LIG-ctl, **(c)** LIG-1300m-alb minus LIG-ctl, and **(d)** LIG-1300m-

alb minus LIG-1300m. Hatched areas mark statistically insignificant TS anomalies.

Figure 3. Effect of Greenland Ice Sheet elevation and albedo on surface temperature in the 130 kyr BP simulation (LIG-1300m-alb simulation. Same as Fig. 2c but for: **(a)** local winter mean (coldest month) and **(b)** local summer mean (warmest month). Violet dashed lines represent the LIG-1300m-alb 50 %-compactness sea ice isoline, violet continuous lines represent the LIG-1300m-alb sea ice edge. Green dashed lines represent the LIG-ctl 50 %-compactness sea ice isoline, green continuous lines represent the LIG-ctl sea ice edge.

Figure 4. Effect of Greenland Ice Sheet elevation, insolation, and albedo at 130 kyr BP relative to preindustrial (PI). Surface temperature (TS) anomalies (in ° C) between the Last Interglacial (LIG, LIG-1300m-alb-CH_4 simulation) and PI (PI simulation) for: **(a)** annual mean, **(b)** local winter mean (coldest month), and **(c)** local summer mean (warmest month). Violet dashed lines represent the LIG 50 %-compactness sea ice isoline, violet continuous lines represent the LIG sea ice edge. Green dashed lines represent the PI 50 %-compactness sea ice isoline, green continuous lines represent the PI sea ice edge. Hatched areas mark statistically insignificant TS anomalies.

Figure 5. Simulated surface temperature evolution (in °C) for the Last Interglacial (LIG, 130–115 kyr BP, LIG-ctl-tr, LIG-×0.5-tr, LIG-1300m-alb-tr, and LIG-GHG-tr simulations) and the Holocene (8–0 kyr BP, HOL-tr simulation) in northern high latitudes (60–90°N) calculated as running average with a window length of 21 model years representing 210 calendar years for: **(a)** annual mean, **(b)** local winter mean (coldest month), and **(c)** local summer mean (warmest month). The lower *x* scale represents the LIG time scale, the upper *x* scale indicates the Holocene time scale. The upper *x* scale is matched to the time scale between 128 and 120 kyr BP, as Drysdale et al. (2009) propose that Termination I and Termination II are similar with respect to obliquity.

Figure 6. Effect of **(a, b)** Greenland Ice Sheet elevation, insolation, albedo, and atmospheric methane concentration and **(c, d)** insolation and atmospheric methane concentration for the Last Interglacial (LIG) relative to preindustrial (PI). Model-data comparison of mean local summer temperature anomalies (in °C). The shading represents the simulated surface temperature (TS) anomalies at **(a, c)** 130 kyr BP derived from **(a)** LIG- 1300 m-alb simulation and **(c)** LIG-ctl simulation, and **(b, d)**

summer maximum LIG warmth (warmest 100 warmest months between 130 and 120 kyr BP) derived from **(b)** LIG-1300m-alb-tr simulation and **(d)** LIG-ctl-tr, relative to PI. Hatched areas in **(a, c)** mark statistically insignificant TS anomalies. The squares and circles show marine and terrestrial proxy-based maximum LIG summer temperature anomalies relative to PI derived by CAPE Last Interglacial Project Members (2006). The colors inside the squares and circles represent the proxy-based temperature anomalies derived from the intervals provided by CAPE Last Interglacial Project Members (2006), that agree best with the simulated TS anomalies at the location of the proxies.

Figure 7. Effect of **(a, b)** Greenland Ice Sheet elevation, insolation, albedo, and atmospheric methane concentration and **(c, d)** insolation and atmospheric methane concentration for the Last Interglacial (LIG) relative to preindustrial (PI). Model-data comparison of mean annual temperature anomalies (in °C). The shading represents the simulated surface temperature (TS) anomalies at **(a, c)** 130 kyr BP derived from **(a)** LIG-1300m-alb simulation and **(c)** LIG-ctl simulation, and **(b, d)** maximum LIG warmth (warmest 100 model years between 130 and 120 kyr BP) derived from **(b)** LIG-1300m-alb-tr simulation and **(d)** LIG-ctl-tr simulation, relative to PI. Hatched areas in **(a, c)** mark statistically insignificant TS anomalies. The squares and circles show marine and terrestrial proxy-based LIG annual mean temperature anomalies relative to present-day (1961–1990) derived by Turney and Jones (2010).

Figure 8. Effect of Greenland Ice Sheet elevation, insolation, albedo, and atmospheric methane concentration for the Last Interglacial (LIG) relative to preindustrial (PI). **(a)** Proxy-based maximum LIG summer temperature anomalies (in °C) relative to PI derived by CAPE Last Interglacial Project Members (2006) plotted against simulated local summer surface temperature (TS) anomalies at 130 kyr BP (LIG-1300m-alb simulation) relative to PI at the location of the proxies. The horizontal bars represent the proxy-based temperature intervals derived by CAPE Last Interglacial Project Members (2006). The vertical bars indicate the simulated TS anomalies at the maximum and minimum LIG TS with respect to local summer (i.e. the coldest and warmest 100 warmest months) derived from the time interval 130 to 120 kyr BP (LIG-1300m-alb-tr simulation) relative to PI, for each given proxy record location. **(b)** Proxy-based LIG annual mean temperature anomalies relative to present-day (1961–1990) derived by Turney and Jones (2010), plotted against simulated annual mean TS anomalies at 130 kyr BP(LIG-1300m-alb simulation) relative to PI at the location of the proxies. The vertical bars indicate

the simulated TS anomalies at the maximum and minimum LIG TS with respect to annual mean (i.e the coldest and warmest 100 model years) derived from the time interval 130 to 120 kyr BP (LIG-1300m-alb-tr simulation) relative to PI, for each given proxy record location. **(c)** Same as **b)** but displaying vertical bars that represent local summer and local winter mean (i.e. the warmest 100 warmest months and coldest 100 coldest months). The squares (red) and circles (black) represent marine and terrestrial proxy-based temperature anomalies, respectively. The solid thick lines represent the 1 : 1 line that indicates a perfect match of simulated and reconstructed anomalies.

Figure 9. Timing of the maximum Last Interglacial warmth (in kyr BP) for: **(a)** local summer (warmest 100 warmest months) and **(b)** annual mean (warmest 100 model years) derived from the LIG-1300m-alb-tr simulation, between 130 and 120 kyr BP.

Figure 10. Effect of **(a, b)** Greenland Ice Sheet elevation, insolation, albedo, and atmospheric methane concentration and **(c, d)** insolation and atmospheric methane concentration at 130 kyr BP relative to preindustrial (PI). Model-data comparison of mean local summer temperature anomalies (in °C). The shading represents the simulated surface temperature (TS) anomalies derived from **(a, b)** LIG- 1300 m-alb simulation and **(c, d)** LIG-ctl simulation. Hatched areas mark statistically insignificant TS anomalies. The squares show marine proxy-based LIG summer temperature anomalies relative to present-day derived by Capron et al (2014).

Figure 11. Effect of **(a–c)** Greenland Ice Sheet elevation and **(c)** albedo on sea level pressure (SLP) and surface winds in 130 kyr BP simulations. The shading represents December-January-February (DJF) mean SLP anomalies (in Pa), superimposed by DJF mean surface wind anomalies (in ms^{-1}) for: **(a)** LIG-×0.5 minus LIG-ctl, **(b)** LIG-1300m minus LIG-ctl, and **(c)** LIG-1300m-alb minus LIG-ctl simulations. The vector length indicates the wind speed (in ms^{-1}).

1

Simulation	Time (kyr BP)	CO_2 (ppmv)	CH_4 (ppbv)	N_2O (ppbv)	Greenland Ice Sheet	Veg.	e	ε (°)	ω (°)
LIG-ctl	130	278	650	270	PI	dyn.	0.0382	24.24	49.1
LIG-×0.5	130	278	650	270	×0.5	dyn.	0.0382	24.24	49.1
LIG-1300m	130	278	650	270	-1300m	dyn.	0.0382	24.24	49.1
LIG-1300m-alb	130	278	650	270	-1300m+alb	dyn.	0.0382	24.24	49.1
LIG-1300m-alb-CH_4	130	280	760	270	-1300m+alb	dyn.	0.0382	24.24	49.1
LIG-GHG*	130	257	512	239	PI	PI	0.0382	24.24	49.1
LIG-125k*	125	278	650	270	-1300m+alb	dyn.	0.0400	23.79	128.1
PI	0	280	760	270	PI	dyn.	0.0167	23.45	282.2
LIG-ctl-tr	130-115	278	650	270	PI	dyn.	varying	varying	varying
LIG-×0.5-tr	130-115	278	650	270	×0.5	dyn.	varying	varying	varying
LIG-1300m-alb-tr	130-115	278	650	270	-1300m+alb	dyn.	varying	varying	varying
LIG-GHG-tr	130-115	varying	varying	varying	PI	PI	varying	varying	varying
HOL-tr	8-0	278	650	270	PI	dyn	varying	varying	varying

Table 1

1

		Annual mean TS (°C)			Winter mean TS (°C)			Summer mean TS (°C)		
Simulation	AMOC (Sv)	global	NH	SH	global	NH	SH	global	NH	SH
LIG-ctl	12.8	14.77	15.57	13.98	8.76	6.53	10.98	21.00	24.78	17.22
LIG-×0.5	13.3	15.13	16.03	14.22	9.19	7.12	11.25	21.25	25.09	17.41
LIG-1300m	14.8	15.07	15.95	14.18	9.14	7.05	11.22	21.17	24.96	17.39
LIG-1300m-alb	15.0	15.14	16.00	14.29	9.24	7.10	11.37	21.24	25.02	17.46
LIG-1300m-alb-CH_4	14.4	15.32	16.34	14.29	9.40	7.49	11.31	21.43	25.35	17.50
LIG-GHG	12.8	14.65	15.50	13.80	8.69	6.56	10.82	20.82	24.64	17.00
LIG-125k	14.8	15.19	16.11	14.27	9.46	7.74	11.17	21.20	24.94	17.46
PI	16.3	14.51	15.35	13.67	8.84	7.44	10.23	20.09	22.84	17.33

Table 2

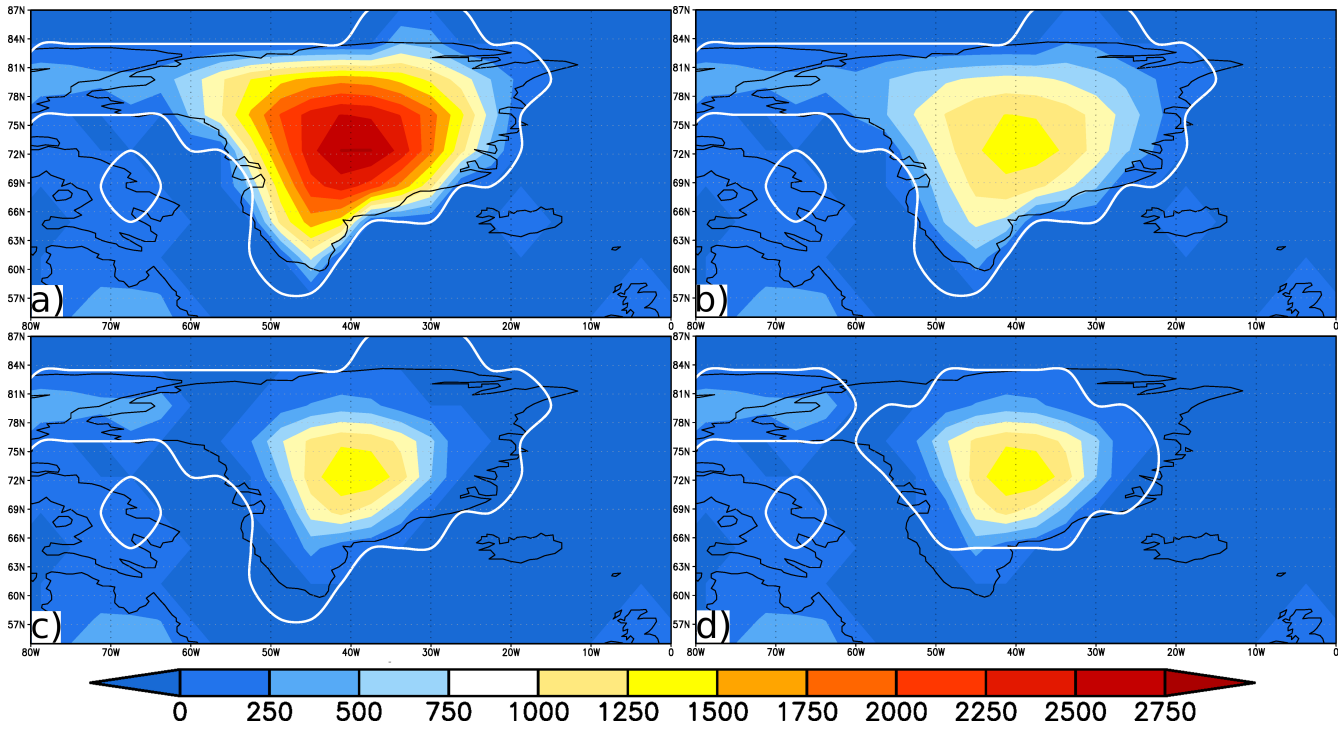
a)
b)
c)
d)
87N
84N
81N
78N
75N
72N
69N
66N
63N
60N
57N
80W
70W
60W
50W
40W
30W
20W
10W
0
0
250
500
750
1000
1250
1500
1750
2000
2250
2500
2750

Figure 1

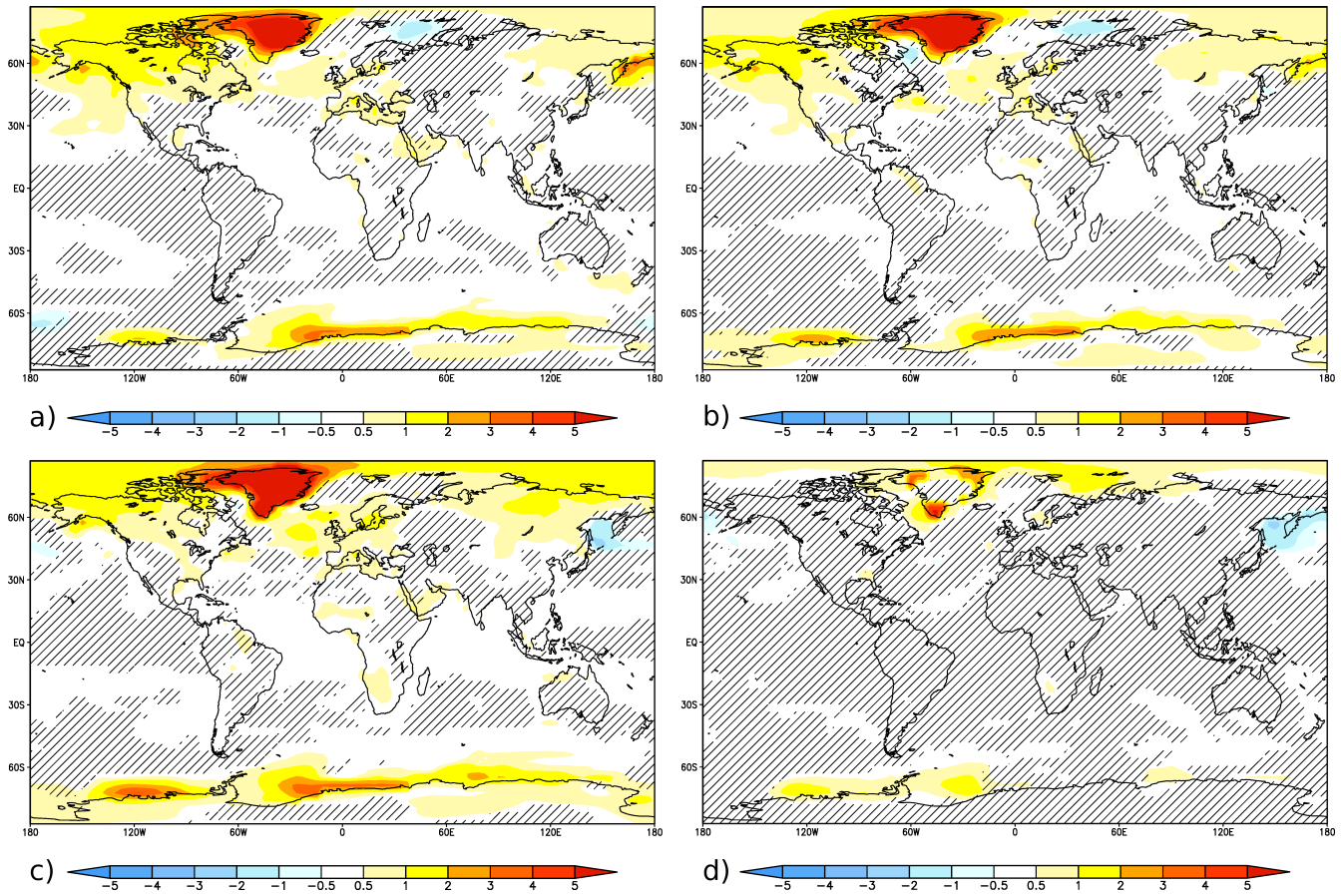
a)
b)
c)
d)
60N
30N
EQ
30S
60S
180
120W
60W
0
60E
120E
180
−5 −4 −3 −2 −1 −0.5 0.5 1 2 3 4 5

Figure 2

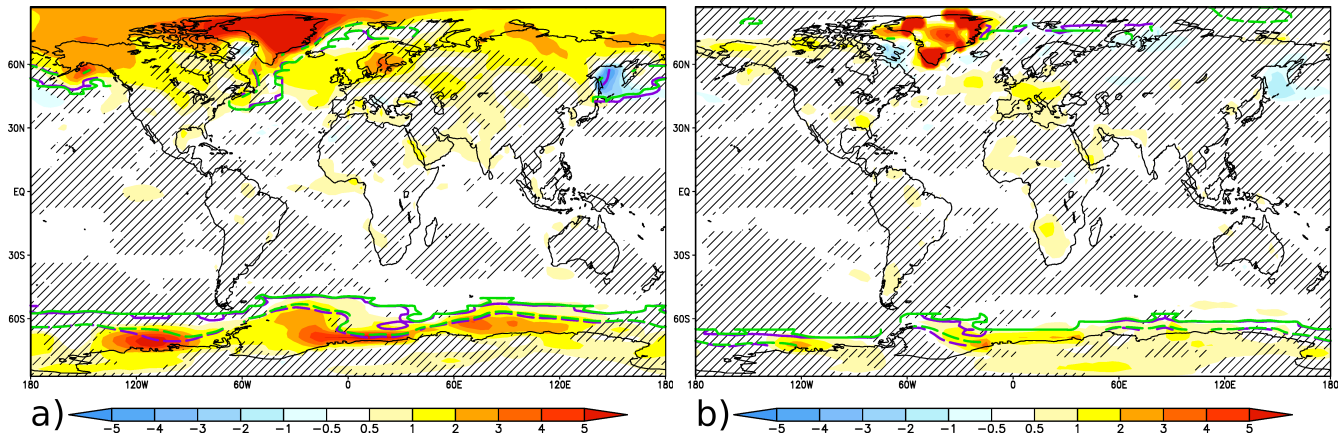
60N
30N
EQ
30S
60S
180
120W
60W
0
60E
120E
180
a)
−5 −4 −3 −2 −1 −0.5 0.5 1 2 3 4 5
b)
−5 −4 −3 −2 −1 −0.5 0.5 1 2 3 4 5

Figure 3

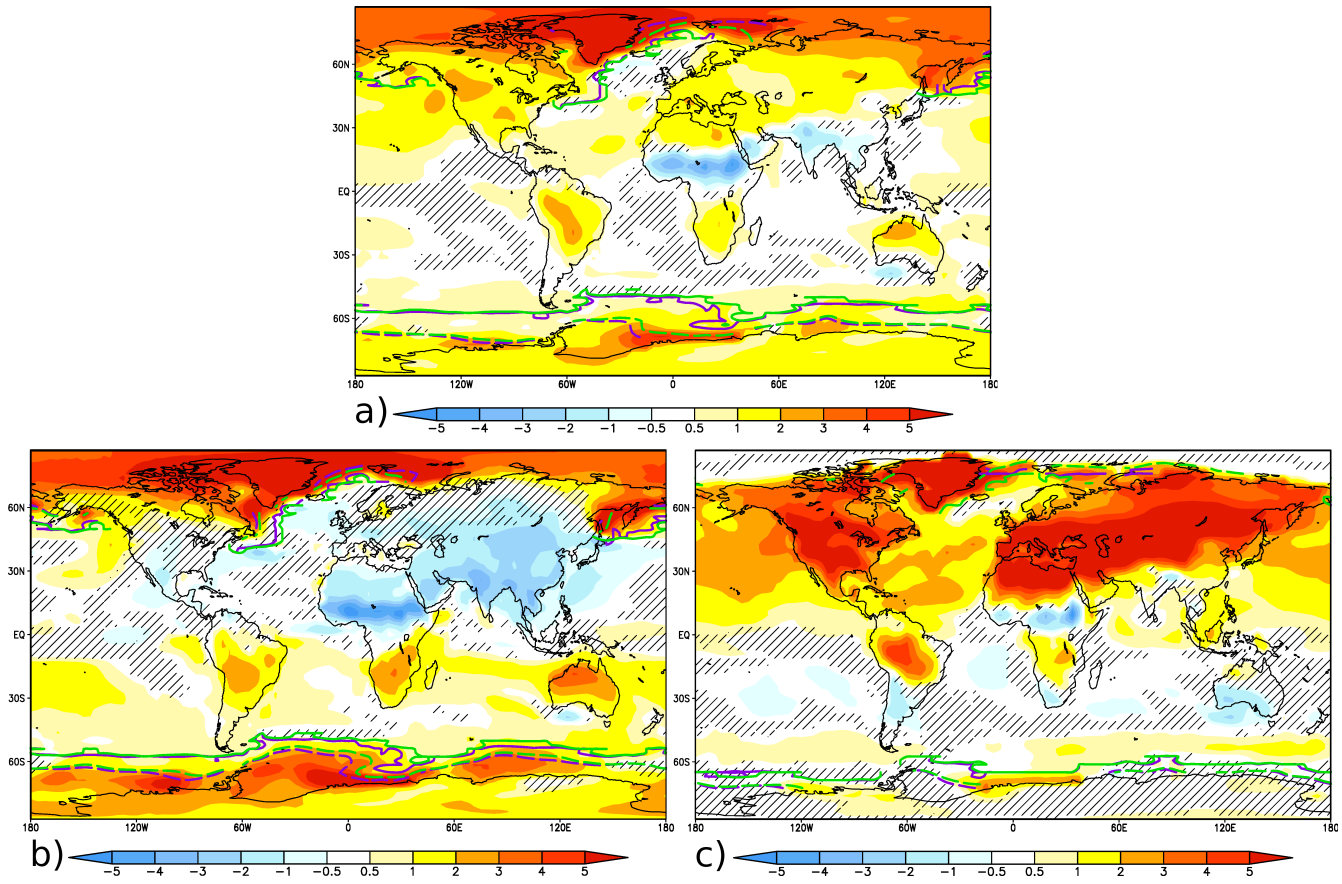
60N
30N
EQ
30S
60S
180
120W
60W
0
60E
120E
180
a)
−5 −4 −3 −2 −1 −0.5 0.5 1 2 3 4 5
b)
c)

Figure 4

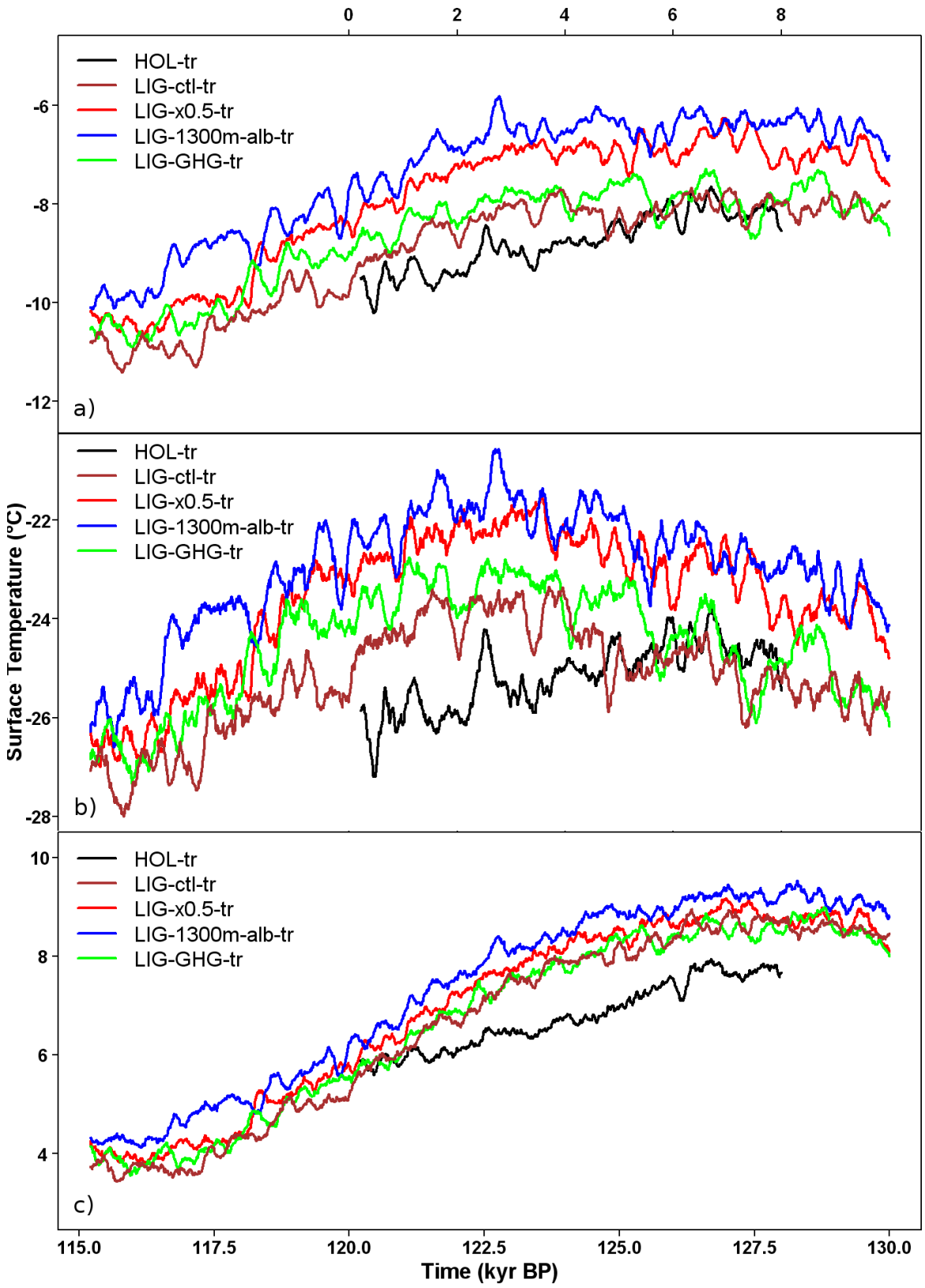
HOL-tr
LIG-ctl-tr
LIG-x0.5-tr
LIG-1300m-alb-tr
LIG-GHG-tr
a)
b)
c)
Surface Temperature (°C)
Time (kyr BP)
0
2
4
6
8
-6
-8
-10
-12
-22
-24
-26
-28
10
8
6
4
115.0
117.5
120.0
122.5
125.0
127.5
130.0

Figure 5

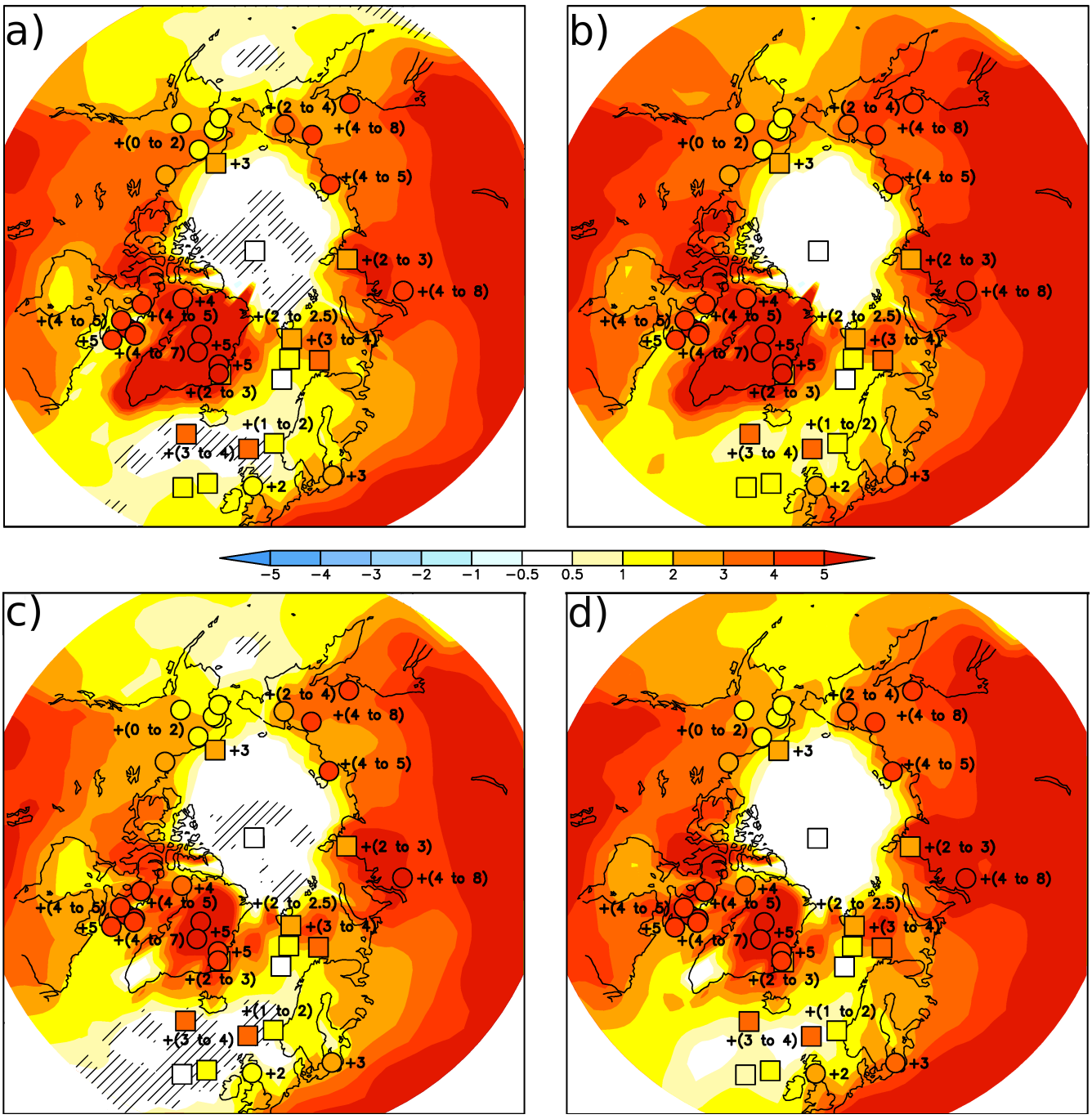
a)
b)
c)
d)
+(0 to 2)
+(2 to 4)
+(4 to 8)
+3
+(4 to 5)
+(2 to 3)
+(4 to 8)
+4
+(4 to 5)
+(2 to 2.5)
+(4 to 5)
+5
+(4 to 7)
+5
+(3 to 4)
+5
+(2 to 3)
+(1 to 2)
+(3 to 4)
+2
+3
−5 −4 −3 −2 −1 −0.5 0.5 1 2 3 4 5

Figure 6

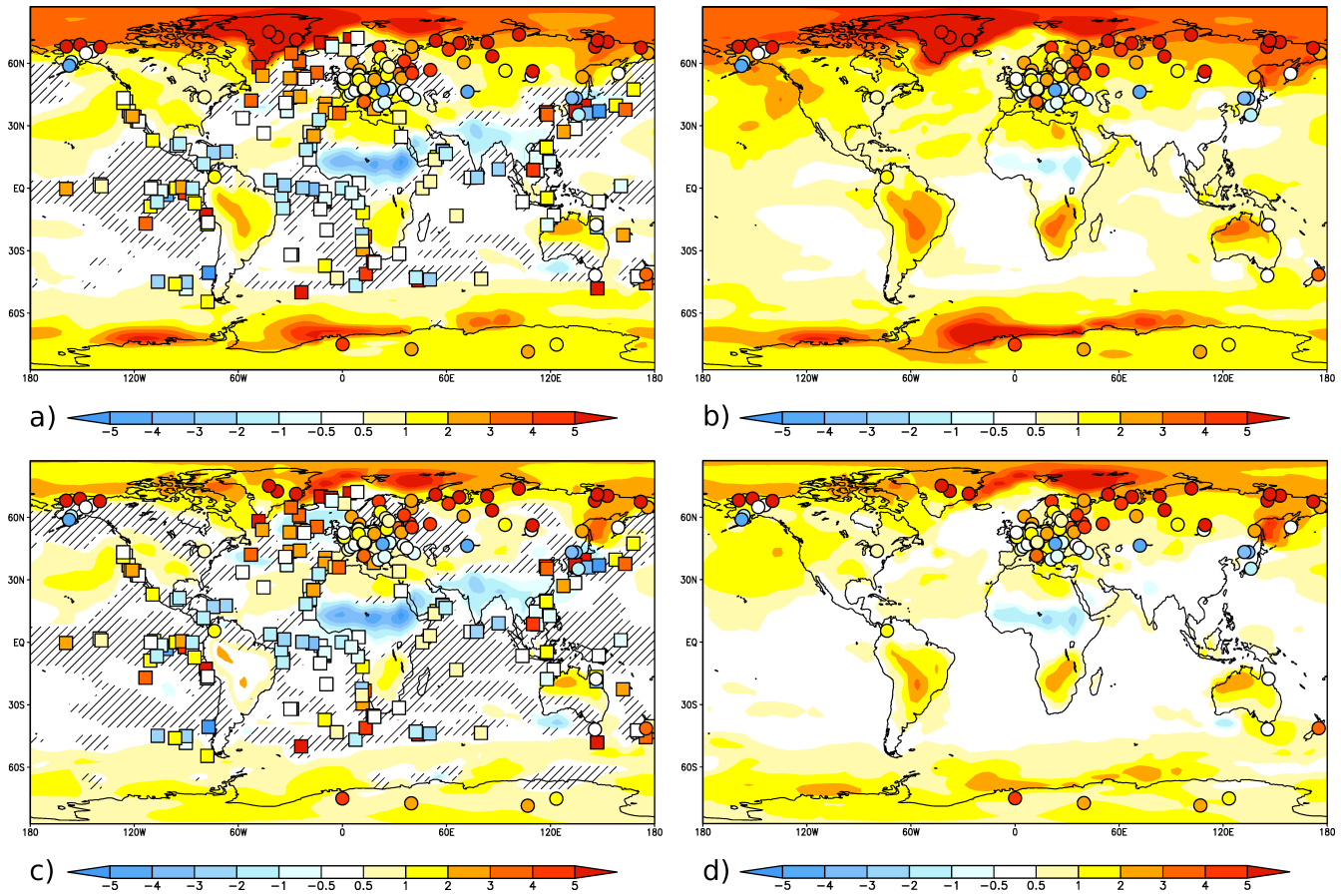
a)
b)
c)
d)
60N
30N
EQ
30S
60S
180
120W
60W
0
60E
120E
180
−5 −4 −3 −2 −1 −0.5 0.5 1 2 3 4 5

Figure 7

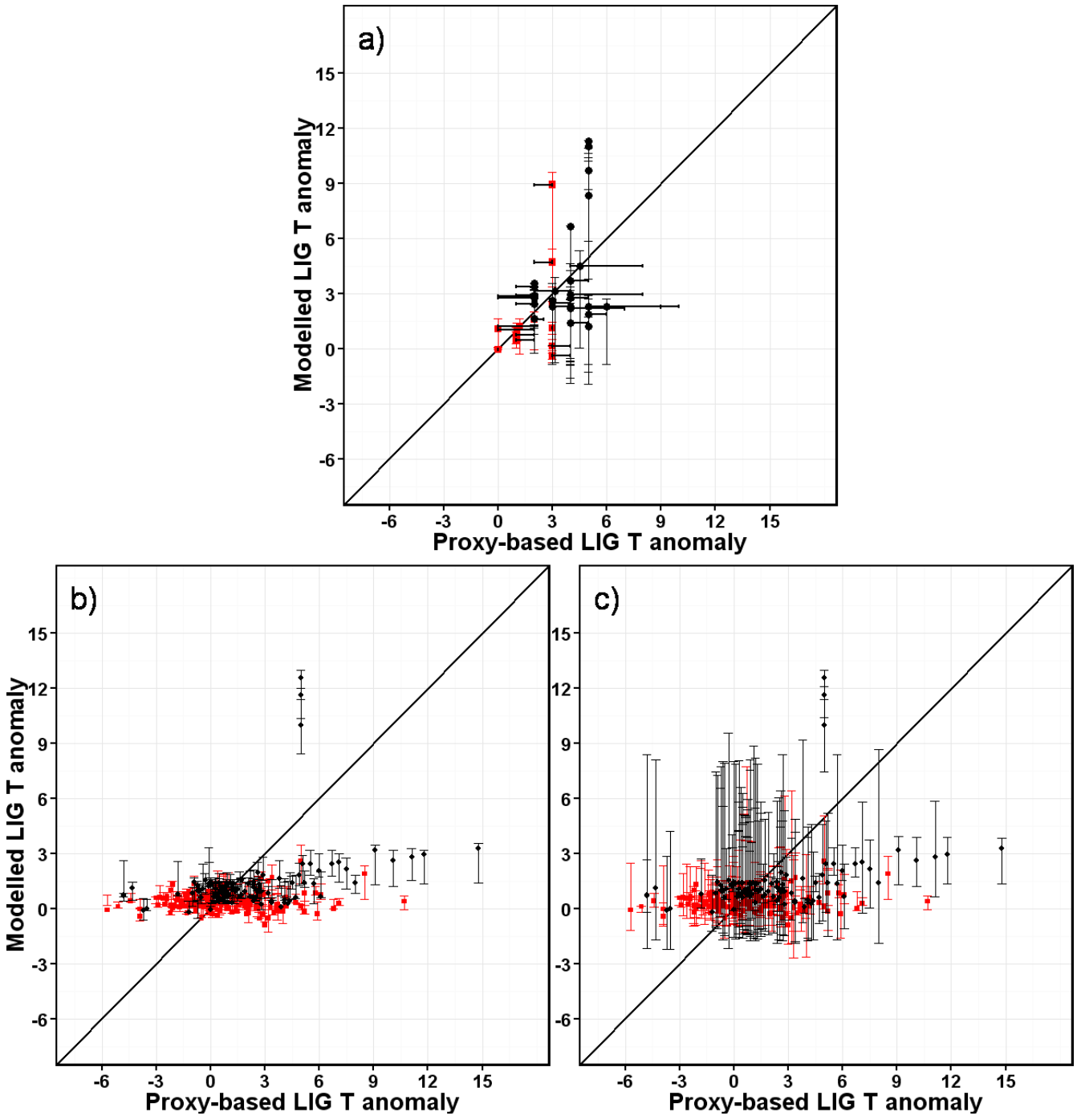
a)
b)
c)
Modelled LIG T anomaly
Proxy-based LIG T anomaly
15
12
9
6
3
0
-3
-6

Figure 8

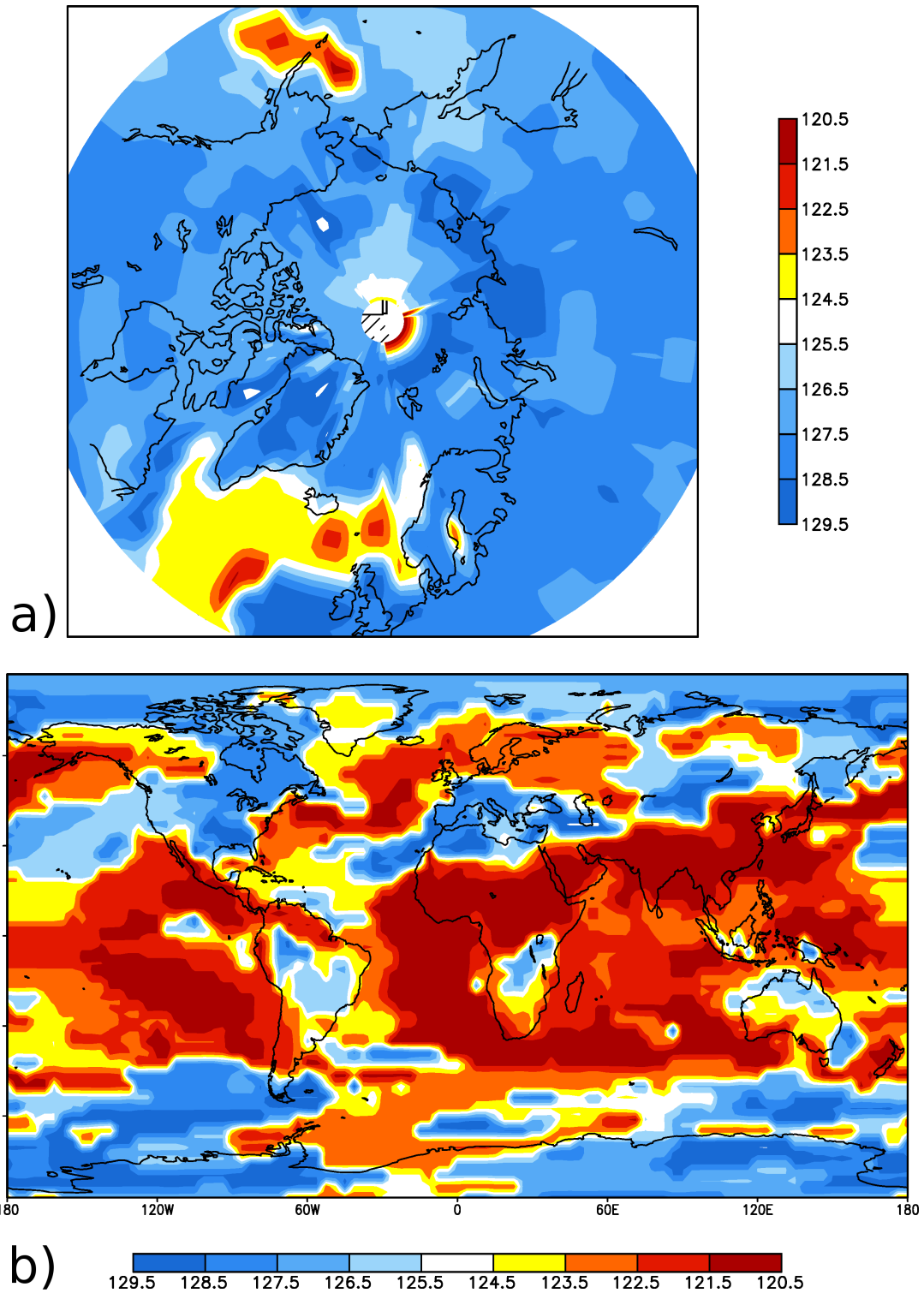
a)
120.5
121.5
122.5
123.5
124.5
125.5
126.5
127.5
128.5
129.5
60N
30N
EQ
30S
60S
180
120W
60W
0
60E
120E
180
b)
129.5
128.5
127.5
126.5
125.5
124.5
123.5
122.5
121.5
120.5

Figure 9

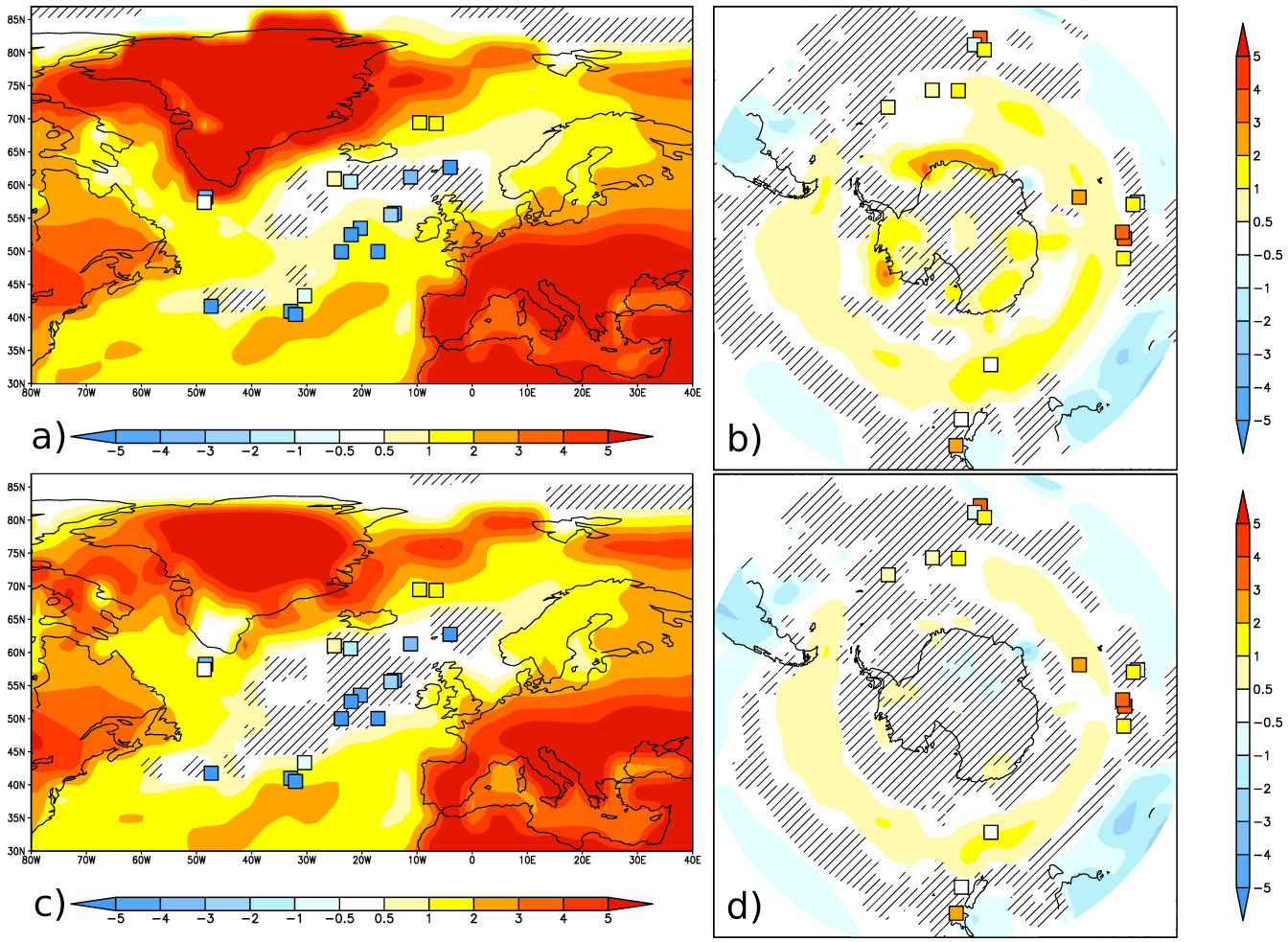
a)
b)
c)
d)
85N
80N
75N
70N
65N
60N
55N
50N
45N
40N
35N
30N
80W
70W
60W
50W
40W
30W
20W
10W
0
10E
20E
30E
40E
−5
−4
−3
−2
−1
−0.5
0.5
1
2
3
4
5

Figure 10

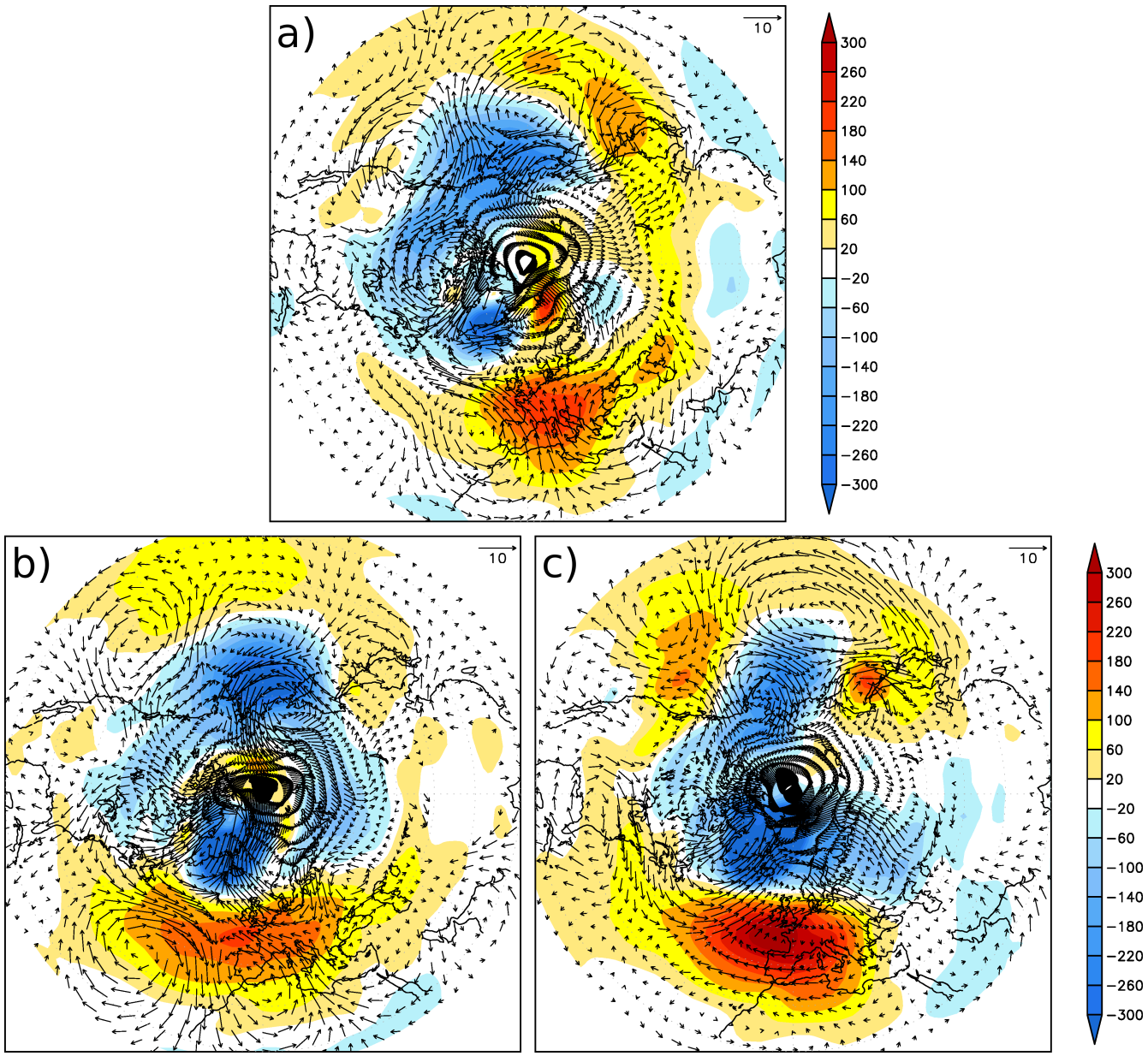
a)
10
300
260
220
180
140
100
60
20
−20
−60
−100
−140
−180
−220
−260
−300
b)
10
c)
10
300
260
220
180
140
100
60
20
−20
−60
−100
−140
−180
−220
−260
−300

Figure 11